

DTIC FILE COPY

2

AD-A226 464

OFFICE OF NAVAL RESEARCH

Grant N00014-90-J-1193

TECHNICAL REPORT No. 22

Semiempirical Study of Rare Gas and Rare Gas-Hydrogen Ionic Clusters:  
 $R_n^+$ ,  $(R_nH)^+$  and  $(R_nH_2)^+$  for R = Ar, Xe

by

Isidore Last and Thomas F. George

Prepared for Publication

in

Journal of Chemical Physics

Departments of Chemistry and Physics  
State University of New York at Buffalo  
Buffalo, New York 14260

August 1990

Reproduction in whole or in part is permitted for any purpose of the  
United States Government.

This document has been approved for public release and sale;  
its distribution is unlimited.

DTIC  
S ELECTE D  
SEP 12 1990  
D CS D

## REPORT DOCUMENTATION PAGE

Form Approved  
OMB No. 0704-0188

1a. REPORT SECURITY CLASSIFICATION Unclassified		1b. RESTRICTIVE MARKINGS	
2a. SECURITY CLASSIFICATION AUTHORITY		3. DISTRIBUTION / AVAILABILITY OF REPORT Approved for public release; distribution unlimited	
2b. DECLASSIFICATION / DOWNGRADING SCHEDULE		4. PERFORMING ORGANIZATION REPORT NUMBER(S) UBUFFALO/DC/90/TR-22	
4. PERFORMING ORGANIZATION REPORT NUMBER(S) UBUFFALO/DC/90/TR-22		5. MONITORING ORGANIZATION REPORT NUMBER(S)	
6a. NAME OF PERFORMING ORGANIZATION Depts. Chemistry & Physics State University of New York	6b. OFFICE SYMBOL (if applicable)	7a. NAME OF MONITORING ORGANIZATION	
6c. ADDRESS (City, State, and ZIP Code) Fronczak Hall, Amherst Campus Buffalo, New York 14260		7b. ADDRESS (City, State, and ZIP Code) Chemistry Program 800 N. Quincy Street Arlington, Virginia 22217	
8a. NAME OF FUNDING / SPONSORING ORGANIZATION Office of Naval Research	8b. OFFICE SYMBOL (if applicable)	9. PROCUREMENT INSTRUMENT IDENTIFICATION NUMBER Grant N00014-90-J-1193	
8c. ADDRESS (City, State, and ZIP Code) Chemistry Program 800 N. Quincy Street Arlington, Virginia 22217		10. SOURCE OF FUNDING NUMBERS	
		PROGRAM ELEMENT NO.	PROJECT NO.
		TASK NO.	WORK UNIT ACCESSION NO.
11. TITLE (Include Security Classification) Semiempirical Study of Rare Gas and Rare Gas-Hydrogen Ionic Clusters: $R_n^+$ , $(R_nH)^+$ and $(R_nH_2)^+$ for $R \equiv Ar, Xe$			
12. PERSONAL AUTHOR(S) Isidore Last and Thomas F. George			
13a. TYPE OF REPORT	13b. TIME COVERED FROM _____ TO _____	14. DATE OF REPORT (Year, Month, Day) August 1990	15. PAGE COUNT 52
16. SUPPLEMENTARY NOTATION Prepared for publication in Journal of Chemical Physics			
17. COSATI CODES		18. SUBJECT TERMS (Continue on reverse if necessary and identify by block number)	
FIELD	GROUP	SUB-GROUP	
			IONIC CLUSTERS RARE GAS HYDROGEN
			SEMIEMPIRICAL STUDY DIATOMICS-IN-IONIC SYSTEMS POLARIZATION FORCES' (73) G
19. ABSTRACT (Continue on reverse if necessary and identify by block number) The ionic rare gas clusters <del>Ar<sub>n</sub><sup>+</sup> and Xe<sub>n</sub><sup>+</sup></del> and rare gas-hydrogen clusters, $(Ar_nH)^+$ , $(Ar_nH_2)^+$ , $(Xe_nH)^+$ and $(Xe_nH_2)^+$ are studied by the semiempirical diatomics-in-ionic-systems (DIIS) method. The $Ar_n^+$ clusters ( $n > 3$ ) are seen to have a structure of a linear $Ar_3^+$ core surrounded by $n-3$ neutral or almost neutral $Ar$ atoms. For $Xe_n^+$ ( $n > 3$ ), a symmetrical $Xe_4^+$ ionic core with the geometry of regular pyramid is formed. The rare gas-hydrogen clusters with one H atom have a simple $R_k(RH)^+$ structure with $k$ neutral rare gas atoms attracted to the $(RH)^+$ molecule by polarization forces. Two H atoms can bind with Ar atoms to form quasistable clusters $Ar_nH_2^+$ which dissociate to $(n-1)Ar + H + (ArH)^+$ through a high barrier of roughly 0.75 eV. Two H atoms and one Xe <sup>+</sup> ion are shown to form a collinear valence-bound $(XeHH)^+$ cluster whose dissociation energy is 0.46 eV.			
20. DISTRIBUTION / AVAILABILITY OF ABSTRACT <input checked="" type="checkbox"/> UNCLASSIFIED/UNLIMITED <input checked="" type="checkbox"/> SAME AS RPT. <input type="checkbox"/> DTIC USERS		21. ABSTRACT SECURITY CLASSIFICATION Unclassified	
22a. NAME OF RESPONSIBLE INDIVIDUAL Dr. David L. Nelson		22b. TELEPHONE (Include Area Code) (202) 696-4410	22c. OFFICE SYMBOL

Semiempirical Study of Rare Gas and Rare Gas-Hydrogen Ionic

Clusters:  $R_n^+$ ,  $(R_nH)^+$  and  $(R_nH_2)^+$  for  $R = Ar, Xe$

Isidore Last\* and Thomas F. George  
Departments of Chemistry and Physics & Astronomy  
239 Fronczak Hall  
State University of New York at Buffalo  
Buffalo, New York 14260

Abstract

The ionic rare gas clusters  $Ar_n^+$  and  $Xe_n^+$  and rare gas-hydrogen clusters  $(Ar_nH)^+$ ,  $(Ar_nH_2)^+$ ,  $(Xe_nH)^+$  and  $(Xe_nH_2)^+$  are studied by the semiempirical diatomics-in-ionic-systems (DIIS) method. The  $Ar_n^+$  clusters ( $n > 3$ ) are seen to have a structure of a linear  $Ar_3^+$  core surrounded by  $n-3$  neutral or almost neutral Ar atoms. For  $Xe_n^+$  ( $n > 3$ ), a symmetrical  $Xe_4^+$  ionic core with the geometry of regular pyramid is formed. The rare gas-hydrogen clusters with one H atom have a simple  $R_k(RH)^+$  structure with  $k$  neutral rare gas atoms attracted to the  $(RH)^+$  molecule by polarization forces. Two H atoms can bind with Ar atoms to form quasistable clusters  $Ar_nH_2^+$  which dissociate to  $(n-1)Ar + H + (ArH)^+$  through a high barrier of roughly 0.75 eV. Two H atoms and one  $Xe^+$  ion are shown to form a collinear valence-bound  $(XeHH)^+$  cluster whose dissociation energy is 0.46 eV.



✓
□
□
Codes
1/ or
st

\* Permanent address: Soreq Nuclear Research Center, Yavne 70600, Israel

A-11

90 0. 006  
9. 00 1. 00

## I. Introduction

The simplest small clusters are formed by (i) rare gas atoms,<sup>1</sup> (ii) rare gas atoms and nonpolar molecules<sup>2-4</sup> and (iii) rare gas atoms and polar molecules.<sup>5-7</sup> In all these clusters, electrons are strongly localized on the component molecules and rare gas atoms such that the particles are bound together only by dispersion (van der Waals) and in case (iii), weak polarization forces. Such clusters are usually called van der Waals (VDW) clusters. The rare gas atoms can also form, however, clusters in which electrons are partly delocalized, contributing to some valence forces between the particles involved. In particular, such delocalization takes place in neutral rare gas-halogen and ionic rare gas clusters.

As an example of neutral rare gas-halogen clusters, we can mention  $\text{Xe}_n\text{Cl}$ . The ground-state  $\text{Xe}_n\text{Cl}$  clusters usually seem to be of the weakly-bound VDW-type. However, ab initio calculations of the  $\text{XeCl}$  complex<sup>8</sup> show that the large electron affinity of the  $\text{Cl}$  atom leads to a small but noticeable electron delocalization which contributes about 50% of the  $\text{XeCl}$  dissociation energy.<sup>9</sup> This delocalization affects the structure of the  $\text{Xe}_n\text{Cl}$  clusters and is responsible for the coupling between their ground state and excited ionic (i.e., charge transfer,  $\text{Xe}_n^+\text{Cl}^-$ ) states.<sup>9</sup> In these excited states the strongly-bound quasistable molecules  $\text{Xe}_2^+\text{Cl}^-$  are formed which have been studied experimentally both in the gaseous<sup>10-12</sup> and solid<sup>13</sup> phases. The  $\text{Xe}_2^+\text{Cl}^-$  molecule can attract more Xe atoms, mainly within Xe solid, forming  $\text{Xe}_n^+\text{Cl}^-$  ( $n > 2$ ) clusters.<sup>9,14-15</sup>

The ionic rare gas clusters  $\text{R}_n^+$  have been studied extensively both experimentally and theoretically. The smallest clusters  $\text{R}_3^+$  have been detected, in particular, in Ar,<sup>16-21</sup> Xe<sup>22</sup> and Kr.<sup>23</sup> Ab initio calculations of  $\text{Ne}_3^+$  and  $\text{Ar}_3^+$ ,<sup>24-25</sup> as well as semiempirical calculations of  $\text{Ar}_3^+$ <sup>26-28</sup> and

$\text{Xe}_3^+$ ,<sup>27,29</sup> show that the triatomic clusters  $\text{R}_3^+$  have a symmetrical linear structure with the central atom bearing roughly 50% of the charge. Clusters with more than three atoms are found for all rare gas atoms, i.e.,  $\text{He}_n^+$ ,<sup>30</sup>  $\text{Ne}_n^+$ ,<sup>31</sup>  $\text{Ar}_n^+$ ,<sup>27,32-36</sup>  $\text{Kr}_n^+$ ,<sup>37</sup> and  $\text{Xe}_n^+$ .<sup>38,39</sup> The large rare gas clusters  $\text{R}_n^+$  with  $n > 10$  demonstrate some magic numbers in their stabilization energy dependence on  $n$ .<sup>33,35,37-43</sup> The structure of the  $\text{R}_n^+$  clusters with  $n > 3$  is not completely clear. According to an experimental study,<sup>35</sup> the  $\text{Ar}_3^+$  ion is the core in the  $\text{Ar}_n^+$  clusters. Theoretical investigations which take into account the electron delocalization support this finding, at least for  $\text{Ar}_n^+$ <sup>26</sup> and  $\text{Xe}_n^+$ ,<sup>29</sup> and show that  $\text{R}_4^+$  ions can also form a core of  $\text{R}_n^+$  ( $n > 4$ ) clusters. The involvement of  $\text{R}_3^+$  and  $\text{R}_4^+$  ions in the  $\text{R}_n^+$  cluster formation allows one to conclude that models with the charge localized on one<sup>33</sup> or two<sup>41,42</sup> centers are unsatisfactory, at least for small  $\text{R}_n^+$  clusters. As shown in Ref. 27 and 29, the charge can be shared even by more than four atoms.

Rare gas atoms can form not only the homonuclear clusters  $\text{R}_n^+$  considered above but also ionic heteronuclear clusters which consist of either different rare gas atoms or rare gas atoms and valence-active atoms. The charge distribution and the structure of heteroatomic ionic clusters depend strongly on the relation between the ionization potentials of the atoms involved. For example, the  $(\text{Xe}_n \text{Ne}_m)^+$  cluster is obviously formed by a  $\text{Xe}_n^+$  ionic core and neutral Ne atoms, since the ionization potential of Ne is much higher than that of Xe. In the case of valence-active atoms such as hydrogen, the situation becomes more complicated because of the formation of the valence-bonded molecules  $\text{H}_2$ ,  $\text{H}_2^+$ ,  $\text{H}_3^+$  and  $(\text{RH})^+$ . The  $(\text{RH}_2)^+$  systems have been studied in the context of the  $\text{R}^+ + \text{H}_2$  and  $\text{R} + \text{H}_2^+$  chemical reactions (see, for example, Refs. 44-46). The  $(\text{ArH}_2)^+$  potential energy surface has been calculated by the DIM method.<sup>47</sup> The study of the rare gas-hydrogen ionic clusters has

concentrated mainly on  $\text{ArH}_3^+$  clusters,<sup>48</sup> whose structure, by analogy with  $\text{HeH}_3^+$ ,<sup>49</sup> has been suggested to be a  $\text{H}_3^+$  triangle with Ar at the vertex. This structure is supported by ab initio calculations.<sup>50</sup> The ionization potential of Ar (15.76 eV) is much higher than that of H (13.6 eV), so that the charge is located on the H atoms. A similar charge distribution is expected for the  $(\text{H}_2)_n\text{H}_3^+$  ionic clusters, which have been studied experimentally,<sup>51</sup> since the ionization potential of  $\text{H}_2$  (15.43 eV) is also much higher than the H ionization potential. Ab initio calculations of rare gas-hydrogen clusters with one H atom have been performed for  $\text{Ne}_n\text{H}^+$  clusters.<sup>52</sup> Due to the large difference between the Ne and H ionization potentials, the charge is strongly localized on  $\text{H}^+$ , and the Ne atoms are bound to  $\text{H}^+$  mainly by polarization forces. A similar situation also occurs for clusters formed by aromatic cations and rare gas atoms. Since the ionization potentials of aromatic molecules are much smaller than those of rare gas atoms, the positive charge is located on the aromatic molecules, which thus attracts the rare gas atoms by polarization forces.<sup>53-55</sup>

The brief survey presented above shows that the study of ionic clusters is a rapidly-developing field of research. Some of the experimental results, especially the discovery of the new (cluster) class of reactions,<sup>56,57</sup> suggest possible practical applications of ionic clusters, such as in catalysis.

In this study we shall present a quantum chemical treatment of the relatively simple ionic clusters  $\text{R}_n^+$ ,  $(\text{R}_n\text{H})^+$  and  $(\text{R}_n\text{H}_2)^+$ . These systems are bound together not only by electrostatic forces but sometimes also by valence forces resulting from the electron (charge) delocalization, as discussed above for  $\text{R}_3^+$  ions. In order to study theoretically the systems with ions where both electrostatic polarization and charge delocalization are of importance, we have previously developed the semiempirical diatomics-in-ionic-systems (DIIS)

method.<sup>9</sup> This method was first applied to rare gas-halogen systems with excited ionic states like  $Xe_n^+Cl^-$ <sup>9,15</sup> and  $Xe_n^+HCl^-$ ,<sup>7</sup> and we shall now use it to calculate the electronic structure of rare gas and rare gas-hydrogen ionic clusters.

In the next section we shall describe briefly the DIIS method, as well as some modifications which one needs to apply it to the systems under consideration. Sections III and IV deal with calculations of  $Ar_n^+$ ,  $(Ar_nH)^+$  and  $(Ar_nH_2)^+$  and of  $Xe_n^+$ ,  $(Xe_nH)^+$  and  $(Xe_nH_2)^+$ , respectively. Section V gives the Conclusions, and the Appendix presents the diatomic potentials.

## II. Diatomics-in-Ionic-Systems (DIIS) Method

### A. Closed-Shell Atoms with Electron Deficiency

Let us consider a polyatomic system  $(A_1A_2\dots A_J)^+$  consisting of J closed-shell atoms or ions  $A_i$  with one electron deficiency (hole) delocalized, generally speaking, between these atoms (ions). For example, the neutral rare gas-halogen system  $R_nX$  is considered in DIIS as  $(R_nX^-)^+$ . The spin of a system with one electron deficiency is  $S = \frac{1}{2}$ . The DIIS wave function is presented as a linear combination of diabatic polyatomic wave functions with localized electron deficiency as<sup>9</sup>

$$\Phi = \sum_{i=1}^J \sum_{m=1}^{M_i} C_{im} \Phi_{im} \quad (1)$$

where  $\Phi_{im}$  is the diabatic wave function of the configuration  $A_1A_2\dots A_{im}^+\dots A_J$ , with the index m indicating the orientation of the  $A_i^+$  open shell ( $M_i = 3$  for a P-symmetry  $A_i^+$  shell). For example,  $R_2X$  is described by nine diabatic

configurations, namely  $R^+RX^-$ ,  $RR^+X^-$  and  $RRX$  for  $m = 1, 2, 3$ . The rare gas ionic cluster  $R_n^+$  is described by  $3n$  diabatic configurations  $R...R^+...R$ . An ionic system consisting of  $n$  rare gas atoms and one hydrogen atom  $(R_nH)^+$  can be also treated by the DIIS method if the electron affinity of H is neglected and singlet states only are considered.<sup>7</sup> The  $(R_nH)^+$  system is described by  $3n + 1$  diabatic configurations, namely  $R...R^+...RH$  ( $m = 1, 2, 3$ ) and  $R...R...RH^+$  ( $m = 1$ ).

The diagonal matrix elements of the DIIS wave function (1) have the physical interpretation as the energies of the diabatic configurations with fixed localization of the electron deficiency. If we consider only the pairwise interactions between atoms (ions), then the diagonal matrix elements are presented as a sum of diatomic interactions,

$$H_{im,im} = \sum_j W_j + \sum_{j_1} \sum_{j_2(>j_1)} W_{j_1j_2} + U_i + \sum_j U_{im,j}, \quad j, j_1, j_2 \neq i \quad (2)$$

where  $W_j$  is the energy of the closed-shell atom  $A_j$ ,  $W_{j_1j_2}$  is the diatomic potential between two closed-shell atoms,  $A_{j_1} - A_{j_2}$ ,  $U_i$  is the energy of atom  $A_i^+$  with an electron deficiency, and  $U_{im,j}$  is the diabatic potential between the closed-shell atom  $A_j$  and the atom with electron deficiency,  $A_i^+$ . The transformation of the potentials between  $m$ -oriented orbitals to the  $\Sigma$  and  $\Pi$  potentials is described in Ref. 9, where the expressions for the off-diagonal matrix elements are given as well. The atom H is considered here as a closed shell atom. In the case of ionic systems, like  $R_n^+$  or  $(R_nH)^+$ , the closed-shell atoms are neutral, and the atoms with electron deficiency are the ions  $R^+$  or  $H^+$ . The diatomic potentials between neutral atoms,  $W_{RR}$  and  $W_{RH}$ , are taken to be known from empirical studies or ab initio calculations. The diabatic

potentials between neutral atoms and ions, such as  $R^+-R$ ,  $R^+-H$ ,  $R-H^+$ , have to be calculated since only adiabatic potentials, such as  $W_{R_2}^+$  and  $W_{(RH)^+}$ , are the physically-defined values.

The diabatic potentials  $U_{i,m,j}$  can be found by considering the diatomic fragments within the DIIS approximation and solving the inverse problem of the  $2 \times 2$  matrix eigenvalues, i.e., calculating the matrix elements for given eigenvalues. In the case of the homonuclear fragment  $R_2^+$ , the  $2 \times 2$  matrix of the fragment is

$$\begin{vmatrix} U - E & V \\ V & U - E \end{vmatrix} = 0 \quad , \quad (3)$$

where  $U$  is the  $R^+-R$  diabatic potential and  $V$  is the exchange term in the  $(R^+R)-(RR^+)$  coupling. Substituting into (3) the known adiabatic potentials  $E^{(1)} = {}^2\Sigma_u$  and  $E^{(2)} = {}^2\Sigma_g$  or  $E^{(1)} = {}^2\Pi_g$  and  $E^{(2)} = {}^2\Pi_u$ , we can easily find the diabatic  $R^+R$  potential  $U$  and the exchange term  $V$  for  $\Sigma$ - or  $\Pi$ -symmetry. For the case of the heteroatomic fragment  $(RH)^+$ , there are two different diabatic potentials,  $U_{R^+H}$  and  $U_{RH^+}$ ,

$$\begin{vmatrix} U_{R^+H} - E & V \\ V & U_{RH^+} - E \end{vmatrix} = 0 \quad . \quad (4)$$

In order to find  $U_{R^+H}$ ,  $U_{RH^+}$  and  $V$  for two given adiabatic potentials, for example,  $E^{(1)} = X^1\Sigma$  and  $E^{(2)} = B^1\Sigma$ , one needs an extra empirical or ab initio value such as the static or transition dipole moment. After the diabatic

potentials  $U_{im,j}$  and the exchange terms  $V_{i_1 m_1, i_2 m_2}$  are determined from Eqs. (3) and (4), the diagonal matrix elements (2) and the off-diagonal matrix elements (presented in Ref. 9) can be calculated, and the wave function (1) and its energy spectrum can be found.

In the wave function presentation (1), the spin-orbit coupling is not taken into account, at least directly. Indirectly, the energy level shifts resulting from the spin-orbit coupling are incorporated into the system energy via the empirical or ab initio diatomic potentials which are used in the DIIS calculations as the input. By neglecting the spin-orbit coupling in the wave function, we are losing some of the excited states and are excluding from our consideration effects such as S-P mixing in collinear configurations.

#### B. Polarization Energy

In applying Eqs. (2)-(4), we need not care about the polarization component of the ion-atom interactions, since it is included in the empirical or ab initio potentials which we are suggesting to use. However, the polarization of atoms gives rise to the electrostatic dipole-dipole interaction which is of three-particle origin (ion-atom-atom) and cannot be considered in a pairwise way. The energy of the dipole-dipole interaction is usually small, although it is not necessarily negligible, and hence we intend to take it into account. Including this energy as a separate term  $\Delta_i$  within the diagonal matrix element (2) and taking as zero the energy of the separated neutral atoms, we obtain

$$H_{im,im} = I_i + \sum_{j_1} \sum_{j_2 (> j_1)} W_{j_1 j_2} + \sum_j U_{im,j} + \Delta_i, \quad j, j_1, j_2 \neq i, \quad (5)$$

where  $I_i$  is the ionization potential of the  $i$ -th atom, and

$$\Delta_i = \sum_{j_1} \sum_{j_2 (> j_1)} \Delta_{i,j_1,j_2} \quad (6)$$

with  $\Delta_{i,j_1,j_2}$  as the dipole-dipole interaction between two neutral atoms polarized by the ion with index  $i$ .<sup>14</sup> Since the terms  $\Delta_{i,j_1,j_2}$  depend on the diatomic polarization energies  $P_{ij}$ , we must calculate them.  $P_{ij}$  are used for the  $\Delta_i$  calculation only, so that their effect is supposedly weak, which reduces significantly the requirements for their accuracy.

In the dipole approximation the ion-atom polarization energy decreases with the fourth power of the separation  $R$ ,

$$P_{ij} = -C_j/R_{ij}^4, \quad C_j = e^2\alpha_j/2 \quad (7)$$

where  $\alpha_j$  is the polarizability of the  $j$ -th atom. The dipole approximation (7) is justified provided that atoms do not overlap one with another. From physical reasons it is clear that the overlap between an ion and atom has a damping effect on the polarization energy  $P_{ij}$ . We suggest taking this account into effect by multiplying the polarizability  $\alpha_j$  in Eq. (7) by a damping function  $\gamma(R_{ij})$ ,

$$\bar{\alpha}_j(R_{ij}) = \alpha_j \gamma(R_{ij}) \quad (8)$$

A suggested form for the functional dependence on  $R_{ij}$  is

$$\gamma(R_{ij}) = \left[ 1 + \left( \frac{r_i + r_j}{R_{ij}} \right)^{12} \right]^{-1/3} \quad (9)$$

where  $r_i$  and  $r_j$  are the ionic and atomic radii, respectively. For the case of the interaction between polarized neutral atoms, both  $r_i$  and  $r_j$  are atomic radii. When the interatomic separation  $R_{ij}$  is larger than the sum of atomic radii (non-overlapping atoms), the function  $\gamma$  is close to unity, i.e., the dipole approximation is valid. When the interatomic separation is smaller than the sum of atomic radii (overlapping atoms), the damping function decreases as  $R_{ij}^4$ , so that the ion-atom polarization energy (7) is saturated with a limiting value of  $-C_j/(r_i+r_j)^4$ . The suggested form (9) for the  $R_{ij}$  dependence is of course arbitrary, but at least it describes in a proper way the asymptotic behavior. If the asymptotic conditions are fulfilled, the form of the dependence of  $\gamma$  on  $R_{ij}$  does not imply much about the results. According to our estimations, different reasonable models of the damping function  $\gamma(R_{ij})$  vary the energy within a range of 0.03 eV only, mostly even much less. For the values  $r_i$  and  $r_j$  in (9), we shall use the atomic VDW radii.

### C. $(R_n H_2)^+$ System

The ionic rare gas-hydrogen system  $(R_n H_2)^+$  is described in the DIIS method as  $n$  closed-shell atoms (R) and two open-shell atoms (H) with one positively-charged hole. Each of the two diabatic configurations  $R \dots R H^+ H$  with a hole located on one of the H atoms is described by a wave function with a fixed  $s = \frac{1}{2}$  spin on the only open-shell atom (H). The situation is much more complicated in the diabatic configuration  $R \dots R^+ \dots R H H$  when the hole is located on one of the  $n$  rare gas atoms. In this configuration there are three open-shell atoms ( $R^+, H, H$ ) with spins  $s = \frac{1}{2}$ , which make two different spin states for a total spin  $S = \frac{1}{2}$ . Consequently, each  $R \dots R^+ \dots R H H$  configuration with fixed hole location is described by six diabatic wave functions which

differ from another not only by p-orbital orientation, like in expansion (1), but also by spin eigenfunctions. Taking into account the hole delocalization between all rare gas and hydrogen atoms, one expresses the DIIS wave function as the superposition of  $6n+2$  diabatic wave functions,

$$\Phi = \sum_{i=1}^n \sum_{m=1}^3 \sum_{k=1}^2 C_{imk} \Phi_{imk} + \sum_{j=1}^2 C_{n+j} \Phi_{n+j} \quad (10)$$

where  $\Phi_{n+j}$  describes the diabatic configuration with the charge on an H atom,  $R \dots RH^+H$ ,  $\Phi_{imk}$  describes the diabatic configuration  $R_{(1)} \dots R_{(i)}^+ \dots R_{(n)} HH$  (the numbers in parentheses are the atomic indices) with the  $m$ -orientation of the  $R_{(i)}^+$  P-shell, and  $k$  indicates the spin configuration of the three ( $R_{(i)}^+, H, H$ ) uncoupled electrons. Following the usual DIM presentation of a triatomic wave function,<sup>47,58</sup> we express the diabatic wave functions in terms of one-electron orbitals as

$$\Phi_{i11} = \frac{1}{\sqrt{2}} (|p_{ix} p_{iy} \bar{p}_{iy} p_{iz} \bar{p}_{iz} s_1 \bar{s}_2| - |p_{ix} p_{iy} \bar{p}_{iy} p_{iz} \bar{p}_{iz} \bar{s}_1 s_2|) \prod_{j(\neq i)}^n \phi_j \quad (11)$$

$$\begin{aligned} \Phi_{i12} = \frac{1}{\sqrt{6}} (2|\bar{p}_{ix} p_{iy} \bar{p}_{iy} p_{iz} \bar{p}_{iz} s_1 s_2| - |p_{ix} p_{iy} \bar{p}_{iy} p_{iz} \bar{p}_{iz} s_1 \bar{s}_2| \\ - |p_{ix} p_{iy} \bar{p}_{iy} p_{iz} \bar{p}_{iz} \bar{s}_1 s_2|) \prod_{j(\neq i)}^n \phi_j \end{aligned} \quad (12)$$

$$\phi_j = |p_{jx} \bar{p}_{jx} p_{jy} \bar{p}_{jy} p_{jz} \bar{p}_{jz}| \quad , \quad j = 1, 2, \dots, n \quad (13)$$

$$\Phi_{n+1} = s_2 \prod_j^n \phi_j \quad , \quad \Phi_{n+2} = s_1 \prod_j^n \phi_j \quad (14)$$

where the bars denote the negative spin orientation,  $p_{ix}$ ,  $p_{iy}$ ,  $p_{iz}$  are the p-orbitals of the  $i$ -th rare gas atom, and  $s_1$  and  $s_2$  are the  $1s$  orbitals of the hydrogen atoms. The index  $m = 1$  in  $\phi_{i11}$  and  $\phi_{i12}$  indicates the  $x$ -orientation of the  $R_{(i)}^+$  shell. The diabatic functions  $\phi_{imk}$  for  $m = 2$  ( $y$ -orientation) and  $m = 3$  ( $z$ -orientation) are expressed by equations similar to Eqs. (11)-(12).

The p-orbitals of the diabatic functions (11)-(13) are oriented along fixed  $x, y, z$ -axes. When the diabatic functions are used to form the H-matrix, the  $x, y, z$  oriented p-orbitals have to be transformed to  $\Sigma$  and  $\Pi$  orientations of diatomic fragments.<sup>9</sup> This transformation for arbitrary located atoms is performed by an S matrix whose elements are

$$S_{ij,x\Sigma} = (x_j - x_i)/R_{ij} \quad , \quad S_{ij,x\Pi} = r_{ij}/R_{ij} \quad , \quad S_{ij,x\pi} = 0 \quad , \quad (15a)$$

$$S_{ij,y\Sigma} = (y_j - y_i)/R_{ij} \quad , \quad S_{ij,y\Pi} = -(x_j - x_i)(y_j - y_i)/(R_{ij}r_{ij}) \quad ,$$

$$S_{ij,y\pi} = (z_j - z_i)/r_{ij} \quad , \quad (15b)$$

$$S_{ij,z\Sigma} = (z_j - z_i)/R_{ij} \quad , \quad S_{ij,z\Pi} = -(x_j - x_i)(z_j - z_i)/(R_{ij}r_{ij}) \quad ,$$

$$S_{ij,z\pi} = -(y_j - y_i)/r_{ij} \quad , \quad (15c)$$

$$r_{ij} = \sqrt{(y_j - y_i)^2 + (z_j - z_i)^2} \quad , \quad (16)$$

where  $x_i$ ,  $y_i$  and  $z_i$  are the  $i$ -th atom coordinates,  $R_{ij}$  is the interatomic separation, and the  $\Pi$ -orientation of the  $R_{(i)}^+$  P-shell is indicated by  $\Pi$  when located in the plane formed by  $\vec{R}_{ij}$  and the  $x$ -axis, and by  $\pi$  when perpendicular

to this plane. We shall also use later the following combinations of the S values:

$$T_{ij,m} = S_{ij,m\Pi}^2 + S_{ij,m\pi}^2 \quad (17a)$$

$$T_{ij,m_1 m_2} = S_{ij,m_1\Pi} S_{ij,m_2\Pi} + S_{ij,m_1\pi} S_{ij,m_2\pi} \quad (17b)$$

Applying both the DIIS<sup>9</sup> and DIM<sup>47,58</sup> approaches and using the diabatic functions (11)-(14), we obtain the  $(6n+2) \times (6n+2)$  H-matrix which we shall simply display without going into the details of its construction. The diagonal matrix element for  $R_{(1)} \dots R_{(i)}^+ \dots R_{(n)} H_{(n+1)} H_{(n+2)}$  is

$$\begin{aligned} H_{imk,imk} = & I_R + \sum_{j_1=1}^{n-1} \sum_{(j_2 > j_1)}^n W_{j_1 j_2} + \sum_{j=1}^n [S_{ij,m\Sigma}^2 U_{ij,\Sigma} + T_{ij,m} U_{ij,\Pi}] \\ & + \sum_{j_1=1}^n \sum_{j=1}^2 W_{j_1, n+j} + \sum_{j=1}^2 [S_{i, n+j, m\Sigma}^2 O_{i, n+j, \Sigma}^{(k)} + T_{i, n+j, m} O_{i, n+j, \Pi}^{(k)}] \\ & + W_{n+1, n+2}^{(k)}, \quad j, j_1, j_2 \neq i, \quad k = 1, 2, \end{aligned} \quad (18)$$

$$O_{i, n+j, \Sigma}^{(1)} = \frac{1}{4} {}^1U_{i, n+j, \Sigma} + \frac{3}{4} {}^3U_{i, n+j, \Sigma} \quad (19a)$$

$$O_{i, n+j, \Sigma}^{(2)} = \frac{3}{4} {}^1U_{i, n+j, \Sigma} + \frac{1}{4} {}^3U_{i, n+j, \Sigma}, \quad (19b)$$

and the same for  $O_{i, n+j, \Pi}^{(k)}$ . In Eqs. (18)-(19),  $I_R$  is the rare gas ionization potential,  $W_{j_1 j_2}$  are the R-R potentials,  $W_{j_1, n+j}$  are the R-H potentials,

$W_{n+1,n+1}^{(k)}$  are the H-H  ${}^1\Sigma$  ( $k=1$ ) and  ${}^3\Sigma$  ( $k=2$ ) potentials,  $U_{ij,m\Sigma}$  and  $U_{ij,m\Pi}$  are the  $R_{(i)}^+ - R_{(j)}$  diabatic potentials, and  ${}^1U_{i,n+j,\Sigma}$  ( ${}^1U_{i,n+j,\Pi}$ ) and  ${}^3U_{i,n+j,\Sigma}$  ( ${}^3U_{i,n+j,\Pi}$ ) are the  $\Sigma$ -symmetry ( $\Pi$ -symmetry)  $R^+ - H$  diabatic potentials in the singlet and triplet states, respectively. The diagonal matrix element for  $R \dots R H_{(n+1)}^+ H_{(n+2)}$  is

$$H_{n+1,n+1} = I_H + \sum_{j_1=1}^{n-1} \sum_{(j_2 > j_1)}^n W_{j_1 j_2} + \sum_{j=1}^n (W_{j,n+2} + U_{n+1,j}) + U_{n+1,n+2} \quad (20)$$

and the same for  $H_{n+3,n+2}$ . In Eq. (20),  $U_{n+1,j}$  are the  $H^+ - R$  diabatic potentials, and  $U_{n+1,n+2}$  is the  $H_{(n+1)}^+ - H_{(n+2)}$  diabatic potential.

The off-diagonal matrix element between two  $R_{(1)} \dots R_{(i)}^+ \dots R_{(n)} H_{(n+1)} H_{(n+2)}$  configurations with different ( $k=1,2$ ) spin orientations are:

$$H_{im_1, im_2} = \frac{\sqrt{3}}{4} \sum_{j=1}^2 (-1)^{j-1} [S_{i,n+j,m\Sigma}^2 ({}^3U_{i,n+j,\Sigma} - {}^1U_{i,n+j,\Sigma}) + T_{i,n+j,m} ({}^3U_{i,n+j,\Pi} - {}^1U_{i,n+j,\Pi})] \quad (21)$$

The off-diagonal matrix elements between two

$R_{(1)} \dots R_{(i)}^+ \dots R_{(n)} H_{(n+1)} H_{(n+2)}$  configurations with different ( $m_1, m_2$ ) orbital orientations are

$$H_{im_1 k, im_2 k} = \sum_{j=1}^n [S_{ij,m_1 \Sigma} S_{ij,m_2 \Sigma} U_{ij,\Sigma} + T_{ij,m_1 m_2} U_{ij,\Pi}]$$

$$+ \sum_{j=1}^2 [S_{i,n+j,m_1\Sigma} S_{i,n+j,m_2\Sigma} O_{ij,\Sigma}^{(k)} + T_{i,n+j,m_1m_2} O_{ij,\Pi}^{(k)}] \quad j = 1 \quad (22)$$

$$H_{im_11,im_22} - H_{im_2,im_21} - \frac{\sqrt{3}}{4} \sum_{j=1}^2 (-1)^{j-1} S_{i,n+j,m_1\Sigma} S_{i,n+j,m_2\Sigma} \\ \times ({}^3U_{i,n+j,\Sigma} - {}^1U_{i,n+j,\Sigma}) + T_{i,n+j,m_1m_2} ({}^3U_{i,n+j,\Pi} - {}^1U_{i,n+j,\Pi}) \quad (23)$$

The off-diagonal matrix elements between the configurations

$R_{(1)} \dots R_{(i_1)}^+ \dots R_n H_{(n+1)} H_{(n+2)}$  and  $R_{(1)} \dots R_{(i_2)}^+ \dots R_n H_{(n+1)} H_{(n+2)}$  are

$$H_{i_1m_11,i_2m_21} - H_{i_1m_12,i_2m_22} - S_{i_1i_2m_1\Sigma} S_{i_2i_1m_2\Sigma} V_{i_1i_2\Sigma} \\ + (S_{i_1i_2m_1\Pi} S_{i_2i_1m_2\Pi} + S_{i_1i_2m_1\pi} S_{i_2i_1m_2\pi}) V_{i_1i_2\pi} \quad (24)$$

$$H_{i_1m_11,i_2m_22} = 0 \quad (25)$$

where  $V_{i_1i_2\Sigma}$  and  $V_{i_1i_2\Pi}$  are the exchange terms of the

$(R_{(i_1)}^+ R_{(i_2)}) - (R_{(i_1)} R_{(i_2)}^+)$  coupling (see Eq. (3)). The off-diagonal matrix elements between the configuration  $R_{(1)} \dots R_{(i)}^+ R_{(n)} H_{(n+1)} H_{(n+1)}$  and the configurations  $R_{(1)} \dots R_{(i)} \dots R_{(n)} H_{(n+1)}^+ H_{(n+2)}$  and  $R_{(1)} \dots R_{(i)} \dots R_{(n)} H_{(n+1)} H_{(n+2)}^+$  are

$$H_{im1,n+j} = -S_{i,n+j,m,\Sigma} V_{i,n+j,\Sigma} \quad j = 1,2 \quad (26)$$

$$H_{im2,n+j} = \sqrt{3}(-1)^{j-1} H_{im1,n+j}, \quad j = 1,2 \quad (27)$$

where  $V_{i,n+j,\Sigma}$  is the exchange term in the  $(R^+H)-(RH^+)$  coupling (see Eq. (4)). The  $\Pi$ -component of the coupling is zero. The off-diagonal matrix element between the configurations  $R_{(1)} \dots R_{(n)} H_{(n+1)}^+ H_{(n+1)}$  and  $R_{(1)} \dots R_{(n)} H_{(n+1)} H_{(n+2)}^+$  is equal to the exchange term of the  $(H^+H)-(HH^+)$  coupling in the  $H_2^+$  molecule (see Eq. (3)),

$$H_{n+1,n+2} = V_{n+1,n+2} \quad (28)$$

When the delocalization of the charge is neglected (i.e., setting the exchange terms  $V$  equal to zero), we obtain for  $R \dots R^+ \dots RHH$  the usual DIM matrix elements.

The diabatic potentials  $U_{ij,\Sigma}$  and  $U_{ij,\Pi}$  of the  $R^+R$  diatomic fragments (Eqs. (18) and (22)), as well as  $U_{n+1,n+2}$  of the  $H^+H$  fragment (Eq. (20)), are found by the inverse solution of Eq. (3), as described in Subsection II.A above. The situation is much more complicated for the diabatic potentials  ${}^1U_{i,n+j,\Sigma}$ ,  ${}^3U_{i,n+j,\Sigma}$  (Eqs. (19), (21) and (23)) and  $U_{n+1,j}$  (Eq. (20)) of the  $R^+H$  and  $RH^+$  diatomic fragments. In our approach, the  $(RH)^+$  diatomic fragment is described by a  $3 \times 3$  matrix which is obtained by removing to infinity all other atoms. Using Eqs. (18), (20), (26) and (27), we have

$$\begin{vmatrix} \frac{1}{4} {}^1U_{i,n+1} + \frac{3}{4} {}^3U_{i,n+1} - E & \frac{\sqrt{3}}{4} ({}^3U_{i,n+1} - {}^1U_{i,n+1}) & V_{i,n+1} \\ \frac{\sqrt{3}}{4} ({}^3U_{i,n+1} - {}^1U_{i,n+1}) & \frac{3}{4} {}^1U_{i,n+1} + \frac{1}{4} {}^3U_{i,n+1} - E & -\sqrt{3} V_{i,n+1} \\ V_{i,n+1} & -\sqrt{3} V_{i,n+1} & U_{n+1,i} - E \end{vmatrix} = 0 \quad (29)$$

where we have simplified the notation by dropping the subscript  $\Sigma$  for the  $(R_{(i)}H_{(n+1)})^+$  fragment. Using the  $(RH)^+$  potentials  ${}^1W_{i,n+1}$  and  ${}^3W_{i,n+1}$  (asymptotic to  $R^+ + H$ ) and  $W_{n+1,i}$  (asymptotic to  $R + H^+$ ) as the eigenvalues  $E^{(1)}$ ,  $E^{(2)}$  and  $E^{(3)}$  for Eq. (29), we can find numerically the diabatic potentials  ${}^1U_{i,n+1}$ ,  ${}^3U_{i,n+1}$  and  $U_{n+1,i}$ . The construction of the exchange term  $V_{i,n+1}$  of the  $(RH)^+$  diatomic fragment was described in Subsection II.A (see Eq. (4)). The diabatic  $\Pi$ -potentials  ${}^1U_{i,n+j,\Pi}$  and  ${}^3U_{i,n+j,\Pi}$  coincide with the adiabatic  ${}^1W_{i,n+j,\Pi}$  and  ${}^3W_{i,n+j,\Pi}$  potentials, since the exchange term  $V_{i,n+j,\Pi}$  is equal to zero. The adiabatic diatomic potentials of the diatomic fragments  $R_2$ ,  $H_2$ ,  $RH$ ,  $R_2^+$ ,  $H_2^+$  and  $(RH)^+$  for  $R = Ar, Xe$  are presented in the Appendix.

### III. Argon and Argon-Hydrogen Ionic Clusters $Ar_n^+$ , $(Ar_nH)^+$ and $(Ar_nH_2)^+$

Considering the structure of rare gas-hydrogen ionic clusters, we have decided to look at Ar and Xe, since they are expected to form different kinds of clusters with H due to the difference in their ionization potentials. Specifically, the Ar ionization potential ( $I_{Ar} = 15.76$  eV) is much higher than the H ionization potential ( $I_H = 13.6$  eV), whereas the Xe ionization potential ( $I_{Xe} = 12.13$  eV) is smaller than that of H, which leads to different charge distributions in the argon-hydrogen and xenon-hydrogen clusters. But before considering the rare gas-hydrogen systems, we shall present the results of calculations on the rare gas ionic clusters  $Ar_n^+$  and  $Xe_n^+$ .

#### A. $Ar_n^+$ Clusters

The results of the calculations of the small ionic clusters  $Ar_3^+$ ,  $Ar_4^+$ ,  $Ar_5^+$  and  $Ar_6^+$  are presented in Table 1 and, partly, in Fig. 1. We shall now compare these results with the known experimental and theoretical results which have been obtained for the  $Ar_n^+$  clusters.

According to experimental studies of the simplest cluster,  $\text{Ar}_3^+$ , its energy of dissociation,  $\text{Ar}_3^+ \rightarrow \text{Ar}_2^+ + \text{Ar}$ , is about 0.2 eV.<sup>17,21,23,59,60</sup> There are two alternative structures of the  $\text{Ar}_3^+$  cluster, namely an asymmetrical  $\text{Ar}_2^+\text{Ar}$  structure with the charge concentrated on  $\text{Ar}_2^+$  and a structure with the charge distributed among all three atoms. In the case of the  $\text{Ar}_2^+\text{Ar}$  structure, where the neutral atom is bound to the  $\text{Ar}_2^+$  molecule by polarization forces, the triangle geometry is expected to be the most stable one.<sup>61</sup> When the charge is delocalized among all three atoms, the exchange interaction contributes significantly to the binding so that the symmetrical linear geometry is expected to be the most stable configuration. The first quantum chemistry calculation, performed by the approximate  $X_\alpha$  method, gave preference to the asymmetrical triangle structure.<sup>62</sup> However, the CI *ab initio* calculations,<sup>24,25</sup> as well as semiempirical calculations,<sup>27,29</sup> found the symmetrical linear configuration to be the most stable one. The experimental spectral data, unfortunately, cannot provide direct evidence about the  $\text{Ar}_3^+$  geometry. The conclusions made by the indirect analysis of the experimental data are contradictory. Whereas some of the experimental works confirm the symmetrical linear  $\text{Ar}_3^+$  structure,<sup>17,35,63</sup> other papers substantiate the asymmetrical  $\text{Ar}_2^+\text{Ar}$  structure, either of triangular<sup>61</sup> or linear<sup>19,64</sup> geometry.

Such discrepancy in the conclusions is due, most probably, from the features of the  $\text{Ar}_3^+$  potential energy surface. Since  $\text{Ar}_3^+$  has a very flat  $\text{Ar}_2^+\text{Ar}$  potential,<sup>19,28,64</sup> the vibrational motion shifts, for the most part, the  $\text{Ar}_3^+$  configuration far away from the equilibrium configuration, thus significantly affecting the electronic transitions. This problem has been considered in detail by Gidea and Amarouche,<sup>28</sup> who calculated the potential energy surfaces of  $\text{Ar}_3^+$  by a method similar to DIIS. A trajectory study performed on these potential energy surfaces shows that the symmetrical linear

$\text{Ar}_3^+$  minimum energy configuration alone provides the spectrum close to the experimental one, if one takes into account the vibrational motion.<sup>28</sup>

In our calculations the triatomic cluster  $\text{Ar}_3^+$  has a symmetrical linear equilibrium configuration, in accord with other calculations.<sup>24-28</sup> The  $\Sigma_k \rightarrow \Sigma_g$  transition energy in the equilibrium configuration is found in our calculations to be equal to 2.26 eV, close to the other theoretical values of 2.36 eV<sup>24</sup> and 2.34 eV.<sup>28</sup> Our  $\Sigma_k \rightarrow \Sigma_g$  transition moment is 8.8 D, compared to the ab initio value of 8.24 D.<sup>24</sup> For the Ar-Ar distance at the equilibrium configuration, our calculation gives  $R = 2.59 \text{ \AA}$ , exactly the same as the semiempirical calculation of Gadea and Amarouche<sup>28</sup> but slightly less than ab initio calculations (2.62  $\text{\AA}$ ).<sup>25</sup> The  $\text{Ar}_3^+ \rightarrow \text{Ar}_2^+ + \text{Ar}$  dissociation energy in our calculation is  $D = 0.203 \text{ eV}$ , close to the experimental values of 0.22 eV<sup>17,61</sup> and  $0.18 \pm 0.05 \text{ eV}$ .<sup>21</sup> Other calculations give values a little bit lower than our dissociation energies, namely, 0.18 eV,<sup>24</sup> 0.16 eV,<sup>25</sup> 0.20 eV<sup>27</sup> and 0.17 eV.<sup>28</sup>

The most stable  $\text{Ar}_4^+$  cluster, according to our calculations, is formed by an  $\text{Ar}_3^+$  ion and almost neutral ( $q = +0.002$ ) Ar atom separated from the nearest charged atom by 3.68  $\text{\AA}$  (see Table 1 and Fig. 1.III). The dissociation energy for the  $\text{Ar}_4^+ \rightarrow \text{Ar}_3^+ + \text{Ar}$  detachment process is found to be equal to  $D = 0.047 \text{ eV}$ , a typical energy of the polarization attraction. Another  $\text{Ar}_4^+$  cluster is found in an asymmetrical linear configuration with one almost neutral ( $q = +0.01$ ) atom separated from the nearest atom of  $\text{Ar}_3^+$  by 3.3  $\text{\AA}$  (see Table I and Fig. 1.V). The dissociation energy of this quasistable configuration is  $D = 0.031 \text{ eV}$ , and the potential barrier of the transition to the most stable configuration (Fig. 1.III) is about 0.001 eV only. In the DIM calculation,<sup>27</sup> the linear configuration with the dissociation energy of 0.043 eV is found to be the most stable one. According to experimental studies,<sup>20,65</sup> the spectrum

of  $\text{Ar}_4^+$  and other small  $\text{Ar}_n^+$  clusters is similar to the  $\text{Ar}_3^+$  spectrum, so that the conclusion is made that the  $\text{Ar}_n^+$  ( $n > 3$ ) clusters have a structure of  $\text{Ar}_3^+\text{Ar}_{n-3}$ . This experimental finding supports our result that  $\text{Ar}_3^+\text{Ar}$  is the most stable structure for the  $\text{Ar}_4^+$  cluster. A similar result is obtained for  $\text{Ar}_5^+$  and  $\text{Ar}_6^+$  (see below). Like in the experimental studies, the spectrum of the most stable  $\text{Ar}_4^+$  cluster is found to be similar to that of  $\text{Ar}_3^+$  (Table 2.III). It consists of two transitions with large transition moments and transition energies close to one another and to the  ${}^2\Sigma_g^+$  excitation energy of  $\text{Ar}_3^+$ , so that they give one absorption band with its center close to that of the  $\text{Ar}_3^+$  absorption. It is interesting to note that in the  $\text{Ar}_4^+$  excitation states a strong charge transfer takes place, which makes it impossible to describe the excited  $(\text{Ar}_4^+)^*$  cluster as an  $(\text{Ar}_3^+)^*\text{Ar}$  structure (Table 2). Save for the transitions which resemble the  ${}^2\Sigma_u^+ \rightarrow {}^2\Sigma_g^+$  transition of  $\text{Ar}_3^+$ , we find also in  $\text{Ar}_4^+$  a low-energy (1.79 eV) transition with a small transition moment of  $\mu = 0.7$  D (Table 2).

In addition to the  $\text{Ar}_4^+$  clusters with the ground-state  $\text{Ar}_3^+\text{Ar}$  structure, we find a quasistable symmetrical configuration with all atoms bearing the same charge of  $q = +0.25$ , (Table 1.IV). In this configuration,  $\text{Ar}_4^+$  has the geometry of a regular pyramid with a separation of 2.836 Å between every two atoms. The energy of this fully-symmetrical structure is only 0.1 eV above the energy of the most stable  $\text{Ar}_4^+$  cluster. The spectrum of the symmetrical  $\text{Ar}_4^+$  cluster is quite different from that of  $\text{Ar}_3^+$ . The transition energy to the three lowest excited states which form a degenerate level is only 1.46 eV, compared to 2.26 eV for the first allowed transition in  $\text{Ar}_3^+$  (Table 2). The symmetrical  $\text{Ar}_4^+$  configuration is separated from the stable  $\text{Ar}_3^+\text{Ar}$  configuration by a high barrier of roughly 0.25 eV.

The  $\text{Ar}_5^+$  and  $\text{Ar}_6^+$  clusters are formed in a similar way as the stable  $\text{Ar}_4^+$  cluster, i.e., by a  $\text{Ar}_3^+$  ion and neutral or almost neutral Ar atoms. The energy of one Ar atom detachment is 0.05 eV for  $\text{Ar}_5^+$  and 0.06 for  $\text{Ar}_6^+$  (Table 1). The  $\text{Ar}_5^+$  and  $\text{Ar}_6^+$  spectra are similar to the spectrum of the stable  $\text{Ar}_4^+$  cluster (Table 2.III). The experimental studies confirm that  $\text{Ar}_3^+$  is an ionic core in small  $\text{Ar}_n^+$  clusters.<sup>35,65</sup> However, in large  $\text{Ar}_n^+$  clusters,  $n \geq 15$ , the  $\text{Ar}_2^+$  molecule was found to be the most stable ionic core.<sup>65-67</sup> The transition from the  $\text{Ar}_3^+$  to  $\text{Ar}_2^+$  core with an increase of cluster size can be explained by the polarization effects. The energy of the neutral atoms polarization by the ionic is slightly larger for the  $\text{Ar}_2^+$  than  $\text{Ar}_3^+$  core because of the difference in their dimension. In small  $\text{Ar}_n^+$  clusters, this difference in polarization energy is small compared to the  $\text{Ar}_3^+$  dissociation energy, and consequently it is not expected to affect the core structure. In large  $\text{Ar}_n^+$  clusters, the polarization energy is close to that in solid Ar where, according to our estimations, the difference between the polarization energies of the  $\text{Ar}_2^+$  and  $\text{Ar}_3^+$  cores lies somewhere between 0.3 and 0.6 eV. This energy difference is larger than the  $\text{Ar}_3^+$  dissociation energy, so that the  $\text{Ar}_2^+$  core may become more stable than the  $\text{Ar}_3^+$  one.

#### B. $(\text{Ar}_n\text{H})^+$ Clusters

The structure of the  $(\text{ArH})^+$  clusters is simple: all of them are formed by an  $(\text{ArH})^+$  ionic molecule and  $n-1$  neutral Ar atoms which are bound to  $(\text{ArH})^+$  by polarization forces (Table 3). Since in the  $(\text{ArH})^+$  molecule the H atom bears more charge than the Ar atom ( $q_{\text{H}} = +0.569$ ), the neutral Ar atoms are located on the H side of the  $(\text{ArH})^+$  ion (Fig. 2). The simplest  $(\text{Ar}_n\text{H})^+$  cluster,  $\text{Ar}(\text{ArH})^+$ , has a bent geometry with the neutral Ar atom at a distance of 2.81 Å from H. In the  $\text{Ar}_2(\text{ArH})^+$ ,  $\text{Ar}_3(\text{ArH})^+$  and  $\text{Ar}_4(\text{ArH})^+$  clusters, the

neutral atoms are located symmetrically around the  $(\text{ArH})^+$  molecular axis at the distances of 2.79 Å, 2.79 Å and 2.84 Å, respectively. In the  $\text{Ar}_6(\text{ArH})^+$  clusters, two of the Ar atoms are more tightly bound to  $(\text{ArH})^+$  than the other four Ar atoms. In the sequence of  $\text{Ar}_k(\text{ArH})^+$  clusters, the H charge increases monotonically with  $k$ . The energy of an Ar atom detachment from an  $\text{Ar}_k(\text{ArH})^+$  cluster is relatively large, varying from 0.09 eV for  $k = 6$  to 0.19 eV for  $k = 3$ . The electronic spectrum of the  $\text{Ar}_k(\text{ArH})^+$  clusters is practically the same as the spectrum of the isolated  $(\text{ArH})^+$  molecule. The  $\text{Ar}_k(\text{ArH})^+$  clusters can probably be detected by studying their rotational spectrum, since the  $\text{Ar}_k(\text{ArH})^+$  dipole moment depends strongly on  $k$  (Table 3).

### C. $(\text{Ar}_n\text{H}_2)^+$ Clusters

The ionization potential of Ar (15.76 eV) is close to the ionization potential of the  $\text{H}_2$  molecule (15.426 eV), which leads to strong coupling between the states  $\text{Ar}^+\text{H}_2$  and  $\text{ArH}_2^+$ . This coupling affects significantly the potential energy surfaces of the  $(\text{ArH}_2)^+$  system, which have been calculated by the DIM method.<sup>47</sup> We shall not consider here the  $(\text{ArH}_2)^+$  potential energy surfaces, i.e., we shall not consider the energy  $E$  as a function of the interatomic distances  $R_{\text{Ar-H}(1)}$ ,  $R_{\text{Ar-H}(2)}$  and  $R_{\text{H-H}}$ , but restrict our task to the study of ionic clusters formed by the Ar atom or atoms and the  $\text{H}_2$  molecule. The calculation of the  $(\text{Ar}_n\text{H}_2)^+$  system is performed by the modified DIIS method described in Subsection II.C above.

The  $(\text{ArH}_2)^+$  clusters can be formed by  $\text{Ar}^+ + \text{H}_2$  (-4.746 eV),  $\text{Ar} + \text{H}_2^+$  (-4.95 eV) and  $\text{H} + (\text{ArH})^+$  (-6.215 eV). It follows that the most stable  $(\text{ArH}_2)^+$  cluster is expected to be formed by the  $(\text{ArH})^+$  molecule and H atom. However, the polarization attraction of the H atom to the  $(\text{ArH})^+$  ion is so

weak that, according to our calculation, no  $(\text{ArH}_2)^+$  cluster can be formed. The ionic  $(\text{ArH}_2)^+$  cluster can be formed in a quasistable configurations only. We find that the quasistable  $(\text{ArH}_2)^+$  cluster with the lowest energy is formed by an almost neutral Ar atom ( $q = 0.02$ ) and the  $\text{H}_2^+$  molecular ion with an H-H separation of 1.05 Å, slightly shorter than in the isolated  $\text{H}_2^+$  (1.06 Å). The Ar atom is located in a plane perpendicular to the  $\text{H}_2^+$  axis at a distance of 2.935 Å from the  $\text{H}_2^+$  center (Fig. 2). The energy of the Ar detachment is relatively large,  $D = 0.193$  eV. The  $\text{ArH}_2^+$  cluster is separated from the stable state of separated  $(\text{ArH})^+$  and H by a high barrier of, roughly, 0.75 eV. The saddle point for the  $\text{ArH}_2^+ \rightarrow \text{H} + (\text{ArH})^+$  dissociation lies in the collinear configuration with the interatomic distances  $R_{\text{H-H}} \approx 1.5$  Å and  $R_{\text{Ar-H}} \approx 1.2$  Å. Unfortunately, in the DIM calculation<sup>47</sup> the geometry of Fig. 2 was not studied so we do not have a comparison for our results.

The  $\text{Ar}_n\text{H}_2^+$  clusters with a few Ar atoms have a structure similar to that of  $\text{ArH}_2^+$  (see Fig. 2 and Table 4). In all of these clusters up to  $n = 5$ , the Ar atoms are located in a plane perpendicular to the  $\text{H}_2^+$  axis at distances of about 3 Å. The energy of the Ar detachment is 0.19-0.2 eV, slowly decreasing with  $n$  for  $n > 2$ . The common charge of the Ar atoms slightly increases with  $n$  reaching  $q = \pm 0.075$  in  $\text{Ar}_5\text{H}_2^+$ . The decrease of the  $\text{H}_2^+$  charge with  $n$  leads to some decrease of the H-H interatomic distance, which is 1.03 Å in  $\text{Ar}_5\text{H}_2^+$ . The larger  $\text{Ar}_n\text{H}_2^+$  clusters ( $n > 5$ ) are expected to be much less stable than the clusters presented in Table 4. The photoabsorption spectrum of the  $\text{Ar}_n\text{H}_2^+$  clusters is very different from the  $\text{H}_2^+$  spectrum, since the lowest excited states are built up by charge transfer to Ar atoms and the formation of  $\text{Ar}_n^+\text{H}_2$  (Table 4).

#### IV. Xenon and Xenon-Hydrogen Clusters $Xe_n^+$ , $(Xe_nH)^+$ and $(Xe_nH_2)^+$

##### A. $Xe_n^+$ Clusters

The results of the calculations of the small ionic clusters  $Xe_3^+$ ,  $Xe_4^+$ ,  $Xe_5^+$  and  $Xe_6^+$  are presented in Table 5 and (partly) in Fig. 3. In our calculations, the triatomic cluster  $Xe_3^+$  has a symmetrical linear structure with 50% of the charge at the central atom, in accord with other calculations.<sup>24,29</sup> Our calculation gives 3.38 Å for the Xe-Xe separation in  $Xe_3^+$ , compared to 3.47 Å<sup>24</sup> and 3.32 Å<sup>29</sup> in other calculations. The  $Xe_3^+ \rightarrow Xe_2^+ + Xe$  dissociation energy in our calculation is  $D = 0.20$  eV, which is 0.07 eV lower than the experimental value of 0.27 eV.<sup>22</sup> Our dissociation energy is almost exactly halfway between the values of 0.12 eV<sup>24</sup> and 0.36 eV<sup>26</sup> obtained in two other calculations. For the  $^2\Sigma_u^+ \rightarrow ^2\Sigma_g^+$  transition energy from the equilibrium point, we obtain  $T = 1.87$  eV, a little bit higher value than in Ref. 24 (1.60 eV).

Our results obtained for  $Xe_n^+$  clusters with  $n > 3$  are quite different from those obtained in Ref. 29. According to our calculations, the most stable  $Xe_4^+$  cluster has a structure of a regular pyramid, like  $Ar_4^+$  (Fig. 1.IV), and the lowest energy quasistable  $Xe_4^+$  cluster has a structure  $Xe_3^+Xe$  with the weakly-charged atom ( $q = 0.014$ ) located to the side of the  $Xe_3^+$  axis (Table 5, Fig. 3). We find also a quasistable linear symmetrical  $Xe_4^+$  cluster which energy lies 0.012 eV above the  $Xe_3^+Xe$ . In contrast to this, in Ref. 29 the most stable  $Xe_4^+$  structure (Xe detachment energy of 0.159 eV) is just the linear symmetrical one. A structure like our regular pyramid (Fig. 3.III) was not found in Ref. 29 at all. We find the collinear  $Xe_4^+$  cluster V to be separated from the bent geometry  $Xe_3^+Xe$  cluster IV by a small barrier of 0.03 eV. The  $Xe_3^+Xe$  cluster IV which can be formed easily as the result of the attachment of Xe to  $Xe_3^+$  (attachment energy of 0.08 eV) is separated by a high

barrier of approximately 0.3 eV from the most stable  $\text{Xe}_4^+$  cluster, III. It follows that the  $\text{Xe}_3^+\text{X}$  cluster can exist for a relatively long time when the temperature is not high.

The clusters  $\text{Xe}_5^+$  and  $\text{Xe}_6^+$  are presented in Table 5 for both the  $\text{Xe}_4^+\text{Xe}_{n-4}$  and  $\text{Xe}_3^+\text{Xe}_{n-3}$  structures. The energy of Xe detachment varies in the interval 0.07-0.11 eV. The binding energy of the attached atoms is derived from polarization forces, since these atoms are almost neutral.

In the family of  $\text{Xe}_3^+\text{Xe}_{n-3}$  clusters (IV, VII and IX in Table 5), the strongest transition is to the excited state similar to  $^2\Sigma_g^+$  of  $\text{Xe}_3^+$ , i.e., with a very small charge on the central  $\text{Xe}_3^+$  atom. In some of these clusters, an important portion of the charge is transferred in this excited state from  $\text{Xe}_3^+$  to the attached atoms, for example,  $q = 0.38$  in the  $\text{Xe}_3^+$  cluster IV. As in the case of the  $\text{Ar}_3^+\text{Ar}_{n-3}$  clusters, the transition energy is not affected much by the charge transfer, so that in the  $\text{Xe}_3^+\text{Xe}_{n-3}$  clusters a strong photoabsorption is expected in the same range as in  $\text{Xe}_3^+$ . In addition to this  $\Sigma_u \rightarrow \Sigma_g$ -like transition, more allowed transitions with smaller transition energy are found in the  $\text{Xe}_3^+\text{Xe}_{n-3}$  clusters (Table 6).

In the symmetrical  $\text{Xe}_4^+$  configuration III, there is threefold degenerate level with an energy of 1.20 eV above the ground state (and a transition moment of 2.7 D). In  $\text{Xe}_4^+\text{Xe}$  and  $\text{Xe}_4^+\text{Xe}_2$ , two of the excited states remain degenerate with almost the same excitation energy as in  $\text{Xe}_4^+$ , whereas the third state excitation energy is lowered by about 0.15 eV. The linear  $\text{Xe}_4^+$  cluster has only one strong transition  $\Sigma_u \rightarrow \Sigma_g$ , whose energy is 1.46 eV, about 0.4 eV less than in  $\text{Xe}_3^+\text{Xe}$ . The differences between the spectra of  $\text{Xe}_4^+$  III (regular pyramid),  $\text{Xe}_3^+\text{Xe}$  IV and  $\text{Xe}_4^+$  V (linear) may help in the experimental search for the most stable  $\text{Xe}_4^+$  cluster.

### B. $(\text{Xe}_n\text{H})^+$ Clusters

As in the case of the  $(\text{Ar}_n\text{H})^+$  clusters, the  $(\text{Xe}_n\text{H})^+$  clusters are formed by the  $(\text{XeH})^+$  molecule which attracts more neutral Xe atoms. Since in the  $(\text{XeH})^+$  molecule the Xe atom bears most of the charge, the neutral Xe atoms are located on the rare gas atom side of  $(\text{XeH})^+$  (Fig. 4). The  $\text{Xe}(\text{XeH})^+$  cluster is found to have a linear geometry with a  $\text{Xe} + (\text{XeH})$  dissociation energy of 0.046 eV, which is much less than the  $\text{Ar}(\text{ArH})^+$  dissociation energy (0.163 eV). The energy of the Xe detachment in the  $\text{Xe}_k(\text{XeH})^+$  clusters varies in the interval 0.04-0.08 eV (Table 7). The charge of H in  $(\text{XeH})^+$  slightly decreases when the number of attached neutral atoms increases. The spectrum of the  $\text{Xe}_k(\text{XeH})^+$  clusters is practically the same as that of isolated  $(\text{XeH})^+$ .

### C. $(\text{Xe}_n\text{H}_2)^+$ Clusters

The most stable  $(\text{Xe}_n\text{H}_2)^+$  clusters are expected to be formed by charged Xe atoms and a neutral  $\text{H}_2$  molecule, since the  $\text{H}_2$  ionization potential is about 3.3 eV higher than that of Xe. The calculation of the simplest,  $(\text{XeH}_2)^+$ , system shows the existence of a strongly-bound cluster with the energy of the  $\text{Xe}^+ + \text{H}_2$  dissociation of  $D = 0.456$  eV. This cluster has a linear geometry with the Xe-H distance of 1.79 Å, 0.18 Å larger than in the  $(\text{XeH})^+$  molecule, and the H-H distance of 0.81 Å, 0.07 Å larger than in  $\text{H}_2$  molecule (Fig. 4). Almost a whole charge is concentrated on the Xe atom ( $q = 0.955$ ), but the valence bond between  $\text{Xe}^+$  and  $\text{H}_2$  is strong. The excitation energies for the allowed transitions (in the equilibrium configuration) are 10.76 eV and 18.56 eV, whereas in  $\text{H}_2$  there is one transition, 19.2 eV, and in  $(\text{XeH})^+$  there are two transitions but with energies of 7.93 eV and 13.3 eV.

The structure of  $(\text{Xe}_n\text{H}_2)^+$  clusters with more than one Xe atom is quite different from that of  $(\text{XeH}_2)^+$  due to the formation of  $\text{Xe}_2^+$  or  $\text{Xe}_3^+$  molecules.

All  $(\text{Xe}_n\text{H}_2)^+$  clusters that we have studied ( $n > 1$ ) have the structure  $\text{Xe}_n^+\text{H}_2$  with a practically neutral  $\text{H}_2$  molecule. In the most stable  $\text{Xe}_2^+\text{H}_2$  cluster, the axis of both molecules are perpendicular to one another (Fig. 4). The dissociation energy of this cluster is 0.084 eV. In the  $\text{Xe}_3^+\text{H}_2$  clusters three Xe atoms form, in contrast to the free  $\text{Xe}_3^+$  cluster, a triangular  $\text{Xe}_3^+$  system with Xe-Xe distances in the interval 3.50-3.58 Å. In one of the  $\text{Xe}_3^+\text{H}_2$  isomers with the  $\text{Xe}_3^+\text{H}_2 \rightarrow \text{Xe}_3^+ + \text{H}_2$  dissociation energy of  $D = 0.108$  eV, the  $\text{Xe}_3^+$  plane is perpendicular to the  $\text{H}_2$  axis with its center located on this axis at 3.08 Å from the  $\text{H}_2$  center. In another isomer ( $D = 0.097$  eV),  $\text{H}_2$  is located in the  $\text{Xe}_3^+$  plane. In contrast to the  $\text{Xe}_k(\text{XeH})^+$  clusters, in  $\text{Xe}_n^+\text{H}_2$  clusters ( $n \geq 2$ ), the valence binding affects to a certain degree the cluster structure.

## V. Conclusions

1. The semiempirical diatomics-in-molecules (DIIS) method<sup>9</sup> proves to be an effective tool to treat rare gas  $\text{R}_n^+$  and rare gas-hydrogen  $(\text{R}_n\text{H})^+$  ionic clusters. The DIIS results obtained for the triatomic  $\text{Ar}_3^+$  and  $\text{Xe}_3^+$  clusters are close to those obtained in other studies.

2. According to our calculation, there are two very different isomers of  $\text{R}_4^+$  clusters. One has the structure of a  $\text{R}_3^+$  ion and almost neutral R atom, whereas the other isomer has the symmetrical geometry of a regular pyramid with all four atoms bearing the same charge. We find the  $\text{Ar}_3^+\text{Ar}$  and the symmetrical  $\text{Xe}_4^+$  clusters to be the most stable isomers, so that  $\text{Ar}_n^+$  ( $n = 4-6$ ) and  $\text{Xe}_n^+$  ( $n = 5,6$ ) to have ionic cores  $\text{Ar}_3^+$  and  $\text{Xe}_4^+$ , respectively. The experimentally detected transition from the  $\text{Ar}_3^+$  to  $\text{Ar}_2^+$  ionic core in large ( $n \geq 15$ )  $\text{Ar}_n^+$  clusters results, most probably from the polarization energy increase.

3. The  $(R_n H)^+$  clusters have the structure of a  $(RH)^+$  molecule and  $n-1$  neutral R atoms. The neutral rare gas atoms are located at the H side of the  $(ArH)^+$  molecule in the  $(ArH)^+ Ar_{n-1}$  clusters and at the Xe side of the  $(XeH)^+$  molecule in the  $(XeH)^+ Xe_{n-1}$  clusters.

4. In order to consider the  $(R_n H_2)^+$  clusters, we have modified the DIIS method by including into the DIIS wave function some DIM components which describe  $^3\Sigma$  and  $^3\Pi$  states of the  $R^+H$  fragments. We find that the  $Xe^+$  ion forms with  $H_2$  molecule a stable ( $D_e = 0.46$  eV) collinear cluster  $(XeHH)^+$  with the strong contribution of valence forces. When more Xe atoms are involved, the cluster is formed by  $Xe_n^+$  ( $n > 1$ ) ion and  $H_2$  molecule which are bound one to another by polarization forces only. In the case of Ar atoms, we do not find any stable ionic  $(ArH_2)^+$  clusters. The quasistable clusters are formed by slightly-charged Ar atoms and  $H_2^+$  ionic molecule.

## VI. Acknowledgments

This research was supported in part by the National Science Foundation under Grant CHE-8922288 and the Office of Naval Research. IL thanks the State University of New York at Buffalo for its hospitality in Summer 1989 when this research was initiated.

## Appendix: Diatomic Potentials and Exchange Terms

The matrix elements within the DIIS method are expressed in terms of the potentials and exchange terms of diatomic fragments (see Sec. II). In the  $R_n^+$ ,  $(R_n H)^+$  and  $(R_n H_2)^+$  ionic clusters considered in this work, there are the following neutral and ionic diatomic fragments:  $R_2$ ,  $H_2$ ,  $RH$ ,  $R_2^+$ ,  $H_2^+$  and  $(RH)^+$ . The potentials of the neutral fragments,  $W_{ij}$ , are used directly in the matrix elements expressions. The adiabatic potentials of the ionic fragments,

$W_{ij}$ , are needed for the calculations of the diabatic potentials  $U_{ij}$  (see Eqs. (3), (4) and (29)). When the heteronuclear fragment  $(RH)^+$  is considered, one needs also the exchange term  $V$  which has to be defined independently from the potentials. The potentials are given in eV and the distances in Å.

#### A. Neutral Fragments $R_2$ , $H_2$ and $RH$

We need the following potentials of the neutral fragments:  ${}^1\Sigma_{RR}$ ,  ${}^1\Sigma_{HH}$ ,  ${}^1\Sigma_{RH}$  and  ${}^3\Sigma_{HH}$  (the last one is for  $(R_nH_2)^+$  only). The  $R_2$  potentials are taken as a sum of a repulsive exponential term and an attractive dispersion term,

$$W_{ArAr}({}^1\Sigma) = 6940 \exp[-3.6R] - 60/R^6, \quad (A.1)$$

which provides the empirical<sup>68</sup> values  $R_e = 3.76$  Å and  $D_e = 0.012$  eV and fits the ab initio potential<sup>69</sup> at small  $R$ , and

$$W_{XeXe}({}^1\Sigma) = 24000 \exp[-3.17R] - 320/R^6, \quad (A.2)$$

which provides the empirical<sup>70</sup> values  $R_e = 4.47$  Å and  $D_e = 0.023$  eV and fits the ab initio potential<sup>71</sup> at small  $R$ .

The ground-state  $H_2$  potential is described by a modified (for large  $R$ ) Morse function,<sup>58</sup>

$$W_{HH}({}^1\Sigma_g) = 4.746 G(G-2)g \quad (A.3)$$

$$G = \exp[-a(R-R_e)] \quad (A.4)$$

$$g = \exp[-b(R-R_e)^3] \quad (A.5)$$

In Eqs. (A.4) and (A.5),  $R_e = 0.7417 \text{ \AA}$ , and the parameters  $a = 1.9446 \text{ \AA}^{-1}$  and  $b = 0.1215 \text{ \AA}^{-3}$  are found by fitting the exact  $H_2$  potential.<sup>72</sup> The accuracy of the fit is generally within 0.05 eV for  $R > 0.53 \text{ \AA}$ . The repulsive  $^3\Sigma$  potential of  $H_2$  is described by an anti-Morse function,

$$W_{HH}(^3\Sigma) = 1.963 G(G-2)g \quad , \quad (A.6)$$

where the G-function parameter is  $a = 1.805 \text{ \AA}^{-1}$  and the g-function parameter is  $b = 0.1215 \text{ \AA}^{-3}$ . The potential (A.6) fits the exact potential.<sup>72</sup>

The RH potential is described by a Lennard-Jones potential with the empirical parameters for ArH of  $R_e = 3.62 \text{ \AA}$  and  $D_e = 4.15 \text{ meV}$ <sup>73</sup> and for XeH of  $R_e = 3.93 \text{ \AA}$  and  $D_e = 6.85 \text{ meV}$ :<sup>74</sup>

$$W_{ArH}(^1\Sigma) = 0.0166 \left[ \left( \frac{3.22}{R} \right)^{12} - \left( \frac{3.22}{R} \right)^6 \right] \quad (A.7)$$

$$W_{XeH}(^1\Sigma) = 0.0274 \left[ \left( \frac{3.5}{R} \right)^{12} - \left( \frac{3.5}{R} \right)^6 \right] \quad (A.8)$$

### B. Ionic Homonuclear Fragments $R_2^+$ and $H_2^+$

We need the following adiabatic potentials of the ionic homonuclear fragments:  $^2\Sigma_u$ ,  $^2\Sigma_g$ ,  $^2\Pi_g$ ,  $^2\Pi_u$  for  $R_2^+$  and  $\sigma_g$ ,  $\sigma_u$  for  $H_2^+$ . The attractive  $^2\Sigma_u$  and  $^2\Pi_g$  potentials of  $R_2^+$  are described as a sum of Morse function and the polarization term  $P$ . For argon these are expressed as

$$W_{(ArAr)}(^2\Sigma_u) = 1.184 G(G-2) + P_{Ar} \quad , \quad R_e = 2.48 \quad , \quad a = 2.0 \quad (A.9)$$

$$W_{(ArAr)}(^2\Pi_g) = 0.025 G(G-2) + P_{Ar} \quad , \quad R_e = 3.2 \quad , \quad a = 2.3 \quad (A.10)$$

$$P_{\text{Ar}} = -11.7 \left[ 1 + \left( \frac{3.8}{R} \right)^{12} \right]^{-1/3} / R^4, \quad (\text{A.11})$$

where  $R_e$  and  $a$  in (A.9) and (A.10) are the parameters of the G-function (A.4), and the number 3.8 in (A.11) is twice the radius of the Ar atom. We assume the  $\text{Ar}^+$  radius to be equal to the neutral Ar radius  $r_{\text{Ar}} = 1.9 \text{ \AA}$ . For xenon we have

$$W_{(\text{XeXe})}^{+(\text{}^2\Sigma_u)} = 1.0 G(G-2) + P_{\text{Xe}}, \quad R_e = 3.22, \quad a = 155 \quad (\text{A.12})$$

$$W_{(\text{XeXe})}^{+(\text{}^2\Pi_g)} = 0.01 G(G-2) + P_{\text{Xe}}, \quad R_e = 3.8, \quad a = 3.0 \quad (\text{A.13})$$

$$P_{\text{Xe}} = -2.91 \left[ 1 + \left( \frac{4.4}{R} \right)^{12} \right]^{-1/3} / R^4. \quad (\text{A.14})$$

The Xe and  $\text{Xe}^+$  radii are both taken as equal to  $r_{\text{Xe}} = 2.2 \text{ \AA}$ , so that twice the double radius in (A.14) is  $4.4 \text{ \AA}$ .

The repulsive potentials of  $R_2^+$  are described by a sum of a polarization term  $P$  and anti-Morse function for the  $\Sigma_g$  state or exponential function for the  $\Pi_u$  state:

$$W_{(\text{ArAr})}^{+(\text{}^2\Sigma_g)} = 0.9 G(G+2) + P_{\text{Ar}}, \quad R_e = 2.48, \quad a = 1.72 \quad (\text{A.15})$$

$$W_{(\text{ArAr})}^{+(\text{}^2\Pi_u)} = 1290 \exp[-2.8R] + P_{\text{Ar}} \quad (\text{A.16})$$

$$W_{(\text{XeXe})}^{+(\text{}^2\Sigma_g)} = 0.78 G(G+2) + P_{\text{Xe}}, \quad R_e = 3.22, \quad a = 1.45 \quad (\text{A.17})$$

$$W_{(\text{XeXe})}^{+(\text{}^2\Pi_u)} = 6.910 \exp[-2.75R] + P_{\text{Xe}}. \quad (\text{A.18})$$

The ground-state potentials (A.9) and (A.12) provide the empirical dissociation energies<sup>75</sup> of  $D_e = 1.24$  eV for  $\text{Ar}_2^+$  and  $D_e = 1.08$  eV for  $\text{Xe}_2^+$ . The excited-state potentials (A.10), (A.13) and (A.15)-(A.18) fit the ab initio potentials of Ref. 75.

The exact ground-state potential  $\sigma_g$  of the  $\text{H}_2^+$  molecular ion<sup>76</sup> has been fit by a Morse function in Ref. 77 (there is a misprint in Ref. 77 on p. 17:  $a = 0.6678$  should be  $a = 0.678$ ). In order to improve the fitting at small  $R$ , we have added a repulsive exponential component to the Morse function. At large  $R$ , the fitting is improved by the  $g$ -function (A.5),

$$W_{(\text{HH})^+}(\sigma_g) = 810.7 \exp[-11.34R] + 2.795 G(G-2)g \quad (\text{A.19})$$

with the following parameters for the  $G$ - and  $g$ -functions:  $R_e = 1.054$  Å,  $a = 1.281$  Å,  $b = 0.0067$  Å<sup>-3</sup>. The accuracy of the fit is within 0.015 eV for  $R > 0.74$  Å. The equilibrium distance of the potential (A.19) is 1.06 Å, slightly larger than the parameter  $R_e$  for the  $G$ - and  $g$ -functions. The dissociation energy of the potential (A.19) is  $D_e = 2.79$  eV. The excited  $\sigma_u$  potential<sup>76</sup> is fit by an anti-Morse potential,

$$W_{(\text{HH})^+}(\sigma_u) = 3.014 G(G+2)g, \quad R_e = 1.054, \quad a = 1.379, \quad b = 0.0067. \quad (\text{A.20})$$

The polarization component of the potentials (A.19) and (A.20) is

$$P_H = -4.8 \left[ 1 + \left( \frac{1.7}{R} \right)^{12} \right]^{-1/3} / R^4, \quad (\text{A.21})$$

where 1.7 is the H radius.

### C. Ionic Heteronuclear Fragment (RH)<sup>+</sup>

In order to find from Eq. (4) or (29) the (RH)<sup>+</sup> diabatic  $\Sigma$  potentials U, one needs three adiabatic potentials, namely  $^1\Sigma$  and  $^3\Sigma$  asymptotic to R<sup>+</sup> + H and  $^1\Sigma$  asymptotic to R + H<sup>+</sup>. The adiabatic potentials are described as a sum of an attractive (Morse) or repulsive (anti-Morse or exponential) potential and the polarization term P. The adiabatic  $\Sigma$  potentials of (ArH)<sup>+</sup> are expressed as follows:

$$W_{(\text{ArH})+(X^1\Sigma)} = 3.157 G(G-2) + P_{\text{Ar}} \quad , \quad R_e = 1.266 \quad , \quad a = 1.94 \quad (\text{A.22})$$

$$W_{(\text{ArH})+(B^1\Sigma)} = 2.75 G(G+2) + P_{\text{H}} + 2.16 \quad , \quad R_e = 1.266 \quad , \quad a = 1.2 \quad (\text{A.23})$$

$$W_{(\text{ArH})+(^3\Sigma)} = 600 \exp[-1.8R] + P_{\text{H}} + 2.16 \quad (\text{A.24})$$

$$P_{\text{Ar}} = 11.7 \left[ 1 + \left( \frac{1.9}{R} \right)^{12} \right]^{-1/3} / R^4 \quad (\text{A.25})$$

$$P_{\text{H}} = 4.8 \left[ 1 + \left( \frac{3.6}{R} \right)^{12} \right]^{-1/3} / R^4 \quad . \quad (\text{A.26})$$

In (A.22) and (A.23),  $R_e$  and  $a$  are the parameters for the G-function (A.4), and in (A.23) and (A.24) the number 2.16 presents the difference between the ionization potentials of Ar and H. In the polarization terms (A.25) and (A.26), 1.9 is the Ar radius and 3.6 is the sum of the Ar and H radii. The ground-state (ArH)<sup>+</sup> equilibrium distance  $R_e = 1.266 \text{ \AA}$  in the potential (A.22) is equal to the experimental value.<sup>78,79</sup> This potential provides the ab

initio dissociation energy  $D_e = 4.055$  eV.<sup>80</sup> The ab initio ground-state potential of Ref. 80 is used to find the parameter  $a$  of (A.22). The excited-state potentials (A.23) and (A.24) are found by fitting the ab initio potentials of Ref. 81. The  $(\text{ArH})^+$  exchange term  $V$  is found from Eq. (4) by fitting the ab initio dipole moment,<sup>80</sup> which is close to the experimental value<sup>81</sup> at the equilibrium point,

$$V = -95.5 R^2 \exp[-2.42R] \quad . \quad (\text{A.27})$$

The adiabatic  $\Sigma$  potentials of  $(\text{XeH})^+$  are as follows:

$$W_{(\text{XeH})^+}(\text{X}^1\Sigma) = 4.03 G(G-2) + P_H \quad , \quad R_e = 1.61 \quad , \quad a = 1.56 \quad (\text{A.28})$$

$$W_{(\text{XeH})^+}(\text{B}^1\Sigma) = 73 \exp[-1.3R] + P_{\text{Xe}} + 1.47 \quad (\text{A.29})$$

$$W_{(\text{XeH})^+}(\text{G}^3\Sigma) = 1.3 G(G+2) + P_H \quad , \quad R_e = 1.61 \quad , \quad a = 1.56 \quad (\text{A.30})$$

$$P_H = -4.8 \left[ 1 + \left( \frac{3.9}{R} \right)^{12} \right]^{-1/3} / R^4 \quad (\text{A.31})$$

$$P_{\text{Xe}} = -2.91 \left[ 1 + \left( \frac{2.2}{R} \right)^{12} \right]^{-1/3} / R^4 \quad . \quad (\text{A.32})$$

In (A.29), 1.47 presents the difference between the ionization potentials of H and Xe. In the polarization terms (A.31) and (A.32), 3.9 is the sum of the Xe and H radii and 2.2 is the Xe radius. The ground-state  $(\text{XeH})^+$  equilibrium distance  $R_e = 1.61$  Å in the potential (A.28) is equal to the experimental value.<sup>82</sup> The potential (A.28) provides the ab initio<sup>83</sup> dissociation energy  $D_e = 4.05$  eV, a value close to the experimental dissociation energy of  $D_e \approx 3.8$  eV.<sup>84</sup> The parameter  $a$  of (A.28) is found by fitting the ab initio potential of Ref. 83. The excited-state potentials (A.29) and (A.30) are found by

fitting the ab initio potentials of Ref. 85. The  $(\text{XeH})^+$  exchange term  $V$  is found from Eq. (4) by fitting the ab initio dipole moment,<sup>83</sup>

$$V = -57.7 R^2 \exp[-2.0 R] \quad . \quad (\text{A.33})$$

The  $\Pi$  potentials of  $(\text{ArH})^+$  are obtained by fitting the ab initio potentials of Ref. 81,

$$W_{(\text{ArH})^+(\text{A}^1\Pi)} = 423 \exp[-3.9R] + P_H + 2.16 \quad (\text{A.34})$$

$$W_{(\text{ArH})^+(\text{A}^3\Pi)} = 90 \exp[-1.2R] + P_H + 2.16 \quad , \quad (\text{A.35})$$

where  $P_H$  is given by (A.26). The  $\Pi$  potentials of  $(\text{XeH})^+$  are obtained by fitting the ab initio potentials of Ref. 85,

$$W_{(\text{XeH})^+(\text{A}^1\Pi)} = 370 \exp[-2.74R] + P_H \quad (\text{A.36})$$

$$W_{(\text{XeH})^+(\text{A}^3\Pi)} = 430 \exp[-2.74R] + P_H \quad , \quad (\text{A.37})$$

where  $P_H$  is given by (A.31).

### References

1. M. Bixon and J. Jornter, *J. Chem. Phys.* 91, 1631 (1989).
2. S. R. Hair, J. I. Cline, C. R. Bieler and K. C. Janda, *J. Chem. Phys.* 90, 2935 (1989).
3. D. D. Evard, J. I. Cline and K. C. Janda, *J. Chem. Phys.* 88, 5433 (1988).
4. D. Eichenauer and R. J. LeRoy, *Phys. Rev. Lett.* 57, 2920 (1986).
5. G. T. Frazer and A. S. Pine, *J. Chem. Phys.* 85, 2502 (1986).
6. T. D. Klots, R. S. Ruoff, C. Chuang, T. Emilsson and H. S. Gutowski, *J. Chem. Phys.* 87, 4383 (1987).
7. I. Last and T. F. George, *J. Chem. Phys.* 89, 3071 (1988).
8. P. J. Hay and T. H. Dunning, Jr., *J. Chem. Phys.* 66, 1306 (1977).
9. I. Last and T. F. George, *J. Chem. Phys.* 87, 1183 (1987).
10. F. K. Tittel, W. L. Wilson, R. E. Stickel, G. Marovski and W. E. Ernst, *Appl. Phys. Lett.* 36, 405 (1980).
11. V. S. Dubov, Y. E. Lapsker, A. N. Samoiloova and L. V. Gurvich, *Chem. Phys. Lett.* 83, 518 (1981).
12. A. W. McCown and J. C. Eden, *J. Chem. Phys.* 81, 2933 (1984).
13. M. E. Fajardo and V. A. Apkarian, *J. Chem. Phys.* 85, 5660 (1986).
14. I. Last and T. F. George, *J. Chem. Phys.* 86, 3787 (1987).
15. I. Last, T. F. George, M. E. Fajardo and V. A. Apkarian, *J. Chem. Phys.* 87, 5917 (1987).
16. W. F. Liu and D. C. Conway, *J. Chem. Phys.* 62, 3070 (1975).
17. D. L. Turner and D. C. Conway, *J. Chem. Phys.* 71, 1899 (1979).
18. C. R. Albertoni, R. Kuhn, H. W. Sarkas and A. W. Castleman, Jr., *J. Chem. Phys.* 87, 5043 (1987).
19. M. J. Deluca and M. A. Johnson, *Chem. Phys. Lett.* 162, 445 (1989).
20. Z. Y. Chen, C. R. Albertoni, M. Hezegawa, R. Kuhn and A. W. Castelman, Jr., *J. Chem. Phys.* 91, 4019 (1980).
21. P. M. Dehmer and S. T. Pratt, *J. Chem. Phys.* 76, 843 (1982).
22. H. Helm, *Phys. Rev. A* 14, 680 (1976).

23. F. C. Fehsenfeld, T. J. Brown and D. L. Albritton, Proc. 31st Gaseous Electronics Conference, Buffalo, New York, 1978; Bull. Am. Phys. Soc. 24, 124 (1979).
24. W. R. Wadt, Appl. Phys. Lett. 38, 1030 (1981).
25. H. U. Böhmer and S. D. Peyerimhoff, Z. Phys. D 4, 195 (1986).
26. J. Hesslich and P. J. Kuntz, Z. Phys. D 2, 251 (1986).
27. P. J. Kuntz and J. Valldorf, Z. Phys. D 8, 195 (1988).
28. F. X. Gadea and M. Amarouche, Chem. Phys. 140, 385 (1990).
29. M. Amarouche, G. Durand and J. P. Malrieu, J. Chem. Phys. 88, 1010 (1988)
30. P. W. Stephens and J. G. King, Phys. Rev. Lett. 51, 1538 (1983).
31. P. Scheier and T. D. Märk, J. Chem. Phys. 87, 5238 (1987).
32. U. Buck and H. Mayer, Phys. Rev. Lett. 52, 109 (1984).
33. I. A. Harris, R. S. Kidwell and J. A. Northby, Phys. Rev. Lett. 53, 2390 (1984).
34. A. J. Stace, J. Chem. Phys. 85, 5774 (1986).
35. K. Hiraoka and T. Mori, J. Chem. Phys. 90, 7143 (1989).
36. T. D. Märk, Z. Phys. D 12, 263 (1989).
37. M. Lezius, P. Scheier, A. Stamatovic and T. D. Märk, J. Chem. Phys. 95, 3240 (1989).
38. O. Echt, K. Sattler and E. Recknagel, Phys. Rev. Lett. 47, 1121 (1981).
39. O. Echt, M. C. Cook and A. W. Castleman, Jr., Chem. Phys. Lett. 135, 229 (1987).
40. E. E. Polymeropoulos and J. Brickmakr, Surf. Sci. 156, 563 (1985).
41. M. Haberland, Surf. Sci. 156, 305 (1985).
42. J. J. Saenz, J. M. Soler and N. Garcia, Surf. Sci. 156, 120 (1985).
43. W. Miehle, O. Kandler, T. Leisner and O. Echt, J. Chem. Phys. 91, 5940 (1989).
44. S. Chapman and R. K. Preston, J. Chem. Phys. 60, 650 (1974)
45. M. Baer and H. Nakamura, J. Chem. Phys. 87, 4651 (1987).

46. C. Rebrion, B. R. Rowe and J. B. Marquette, *J. Chem. Phys.* 91, 6142 (1987).
47. P. J. Kuntz and A. C. Roach, *J. Chem. Soc. Faraday Trans. 2* 68, 259 (1972).
48. M. Bogey, H. Bolvin, C. Demuynck, and J. L. Destombes, *Phys. Rev. Lett.* 58, 988 (1987); M. Bogey, H. Bolvin, C. Demuynck, J. L. Destombes and B. P. K. Eijck, *J. Chem. Phys.* 88, 4120 (1988).
49. C. E. Dykstra, *J. Mol. Struct.* 103, 131 (1983).
50. E. D. Simandiras, J. F. Gaw and N. C. Handy, *Chem. Phys. Lett.* 141, 166 (1987).
51. M. Okumare, L. I. Yeh and Y. T. Lee, *J. Chem. Phys.* 88, 79 (1988).
52. R. L. Matcha and M. B. Milleur, *J. Chem. Phys.* 68, 4748 (1978); 69, 3016 (1978).
53. J. Jortner, U. Even, S. Leutwyler and Z. Berkovitch-Yelin, *J. Chem. Phys.* 78, 309 (1984).
54. N. B. Horin, U. Even and J. Jortner, *J. Chem. Phys.* 91, 331 (1989).
55. H.-Y. Kim and M. W. Cole, *J. Chem. Phys.* 90, 6055 (1989).
56. W. R. Peifer, M. T. Coolbaugh and J. F. Garvey, *J. Phys. Chem.* 93, 4700 (1989).
57. W. R. Peifer and J. F. Garvey, *J. Phys. Chem.* 93, 5906 (1989).
58. I. Last and M. Baer, *J. Chem. Phys.* 75, 288 (1981).
59. R. G. Keesee and A. W. Castleman, Jr., *J. Chem. Phys. Ref. Data* 15, 1011 (1986).
60. K. Norwood, J. H. Guo and C. Y. Ng, *J. Chem. Phys.* 90, 2995 (1989).
61. C. A. Woodward, J. E. Upham, A. J. Stace and J. N. Murrell, *J. Chem. Phys.* 91, 7612 (1989).
62. H. H. Michels, R. H. Hobbs and L. A. Wright, *Appl. Phys. Lett.* 35, 153 (1979).
63. J. T. Snodgrass, C. M. Roehl and M. Bowers, *Chem. Phys. Lett.* 159, 10 (1989).
64. N. E. Levinger, D. Ray, K. K. Murray, A. S. Mullin, C. P. Schulz and W. C. Lineberger, *J. Chem. Phys.* 89, 71 (1988).
65. N. E. Levinger, D. Ray, M. L. Alexander and W. C. Lineberger, *J. Chem. Phys.* 89, 5654 (1988).

66. P. G. Lethbridge and A. J. Stace, *J. Chem. Phys.* 89, 4062 (1988).
67. W. Kamke, J. de Vries, J. Krauss, E. Kaiser, B. Kamke and I. V. Hertel, *Z. Phys. D* 14, 339 (1989).
68. R. A. Aziz and M. J. Slaman, *Mol. Phys.* 58, 679 (1986).
69. A. D. McLean, B. Liu and J. A. Barker, *J. Chem. Phys.* 89, 6339 (1988).
70. J. S. Cohen and R. T. Pack, *J. Chem. Phys.* 61, 2372 (1974).
71. P. A. Christiansen, K. S. Pitzer, Y. S. Lee, J. H. Yates, W. C. Ermler and N. W. Winter, *J. Chem. Phys.* 75, 5410 (1981).
72. W. Kolos and C. C. J. Roothaan, *Rev. Mod. Phys.* 32, 219 (1960).
73. K. T. Tang and J. P. Toennies, *J. Chem. Phys.* 66, 1496 (1977).
74. R. W. Brickes, Jr., B. Lantzsch, J. P. Toennies and K. Wallaschewski, *Faraday Disc. Chem. Soc.* 55, 167 (1973).
75. W. R. Wadt, *J. Chem. Phys.* 68, 402 (1978).
76. D. R. Bates, K. Ledsham and A. L. Steward, *Phil. Trans. Soc. London* 246, 215 (1953).
77. J. S. Slater, Quantum Theory of Molecules and Solids 1. Electronic Structure of Molecules (McGraw-Hill, New York, 1963), pp. 17-18.
78. K. B. Laughlin, G. A. Blake, R. C. Cohen, D. C. Hovde and R. J. Saykally, *Phys. Rev. Lett.* 58, 996 (1987).
79. J. Geersten and G. E. Scuseria, *J. Chem. Phys.* 90, 6486 (1989).
80. P. Rosmus, *Theor. Chim. Acta* 51, 359 (1979).
81. V. Sidis, *J. Phys. B* 5, 1517 (1972).
82. S. A. Rogers, C. R. Brazier and P. F. Bernath, *J. Chem. Phys.* 87, 159 (1987).
83. R. Klein and P. Rosmus, *Z. Naturforsch.* 39a, 349 (1984).
84. D. K. Bohme, G. I. Mackay and H. I. Shift, *J. Chem. Phys.* 73, 4976 (1980).
85. G. A. Gallup and J. Macek, *J. Phys. B* 10, 1601 (1977).

Table 1. Structure of the ionic clusters  $Ar_n^+$  and ionic molecule  $Ar_2^+$ . The distances (R) are in Å, and the energies (E,D) in eV.

N	$Ar_n^+$	Structure <sup>1)</sup>	R <sup>2)</sup>	R <sup>3)</sup>	q <sup>4)</sup>	E	Dissociation Products	D
I	$Ar_2^+$		2.48			-1.240	$Ar^+ + Ar$	1.240
II	$Ar_3^+$	linear	2.59			-1.443	$Ar_2^+ + Ar$	0.203
III	$Ar_4^+$	$(Ar_3^+)_z (Ar)_{xz}$	2.59	3.68	0.002	-1.490	$Ar_3^+ + Ar$	0.047
IV	$Ar_4^+$	regular pyramid	2.836			-1.480	$Ar_2^+ + 2Ar$	0.240
V	$Ar_4^+$	linear	2.59	3.3	0.01	-1.474	$Ar_3^+ + Ar$	0.031
VI	$Ar_5^+$	$(Ar_3^+)_z (Ar_2)_{xy}$	2.59	3.68	0	-1.540	$(Ar_4^+)_{III} + Ar$	0.050
VII	$Ar_5^+$	$(Ar_3^+)_z (Ar_2)_{xz}$	2.59	3.61	0.002	-1.540	$(Ar_4^+)_{III} + Ar$	0.050
VIII	$Ar_5^+$	$(Ar_3^+)_z (Ar_2)_{xz}$	2.59	3.68	0.003	-1.537	$(Ar_4^+)_{III} + Ar$	0.047
IX	$Ar_6^+$	$(Ar_3^+)_z (Ar_2)_{xy} (Ar)_x$	2.59	3.61	0.001	-1.601	$(Ar_5^+)_{VI} + Ar$	0.061

1) The subscripts z, xz, etc. denote the location along an axis or in a plane (see Fig. 1.II-V).

2) Distance between adjacent charged atoms.

3) Distance from a neutral or weakly-charged atom to the nearest charged atom.

4) Common charge of all weakly-charged atoms.

Table 2. Transition energy T in eV and transition moment  $\mu$  in Debyes of the allowed transitions in  $\text{Ar}_3^+$  and  $\text{Ar}_4^+$ . q is the charge distribution in the excited states.

N <sup>1)</sup>	$\text{Ar}_n^+$	T	D	q			
				1	2	3	4
II	$\text{Ar}_3^+$	2.26	8.8	0.5	0	0.5	
III	$\text{Ar}_3^+\text{Ar}$	2.24	6.8	0.30	0.01	0.34	0.35
		2.19	2.3	0.10	0.04	0.24	0.62
		1.79	0.7	0.27	0.37	0.15	0.21
V	$\text{Ar}_4^+$ linear	1.97	8.2	0.24	0.01	0.26	0.49
IV	$\text{Ar}_4^+$ pyramid	1.46	2.1	0.25	0.25	0.25	0.25
		1.46	2.1	0.30	0.30	0.20	0.20
		1.46	2.1	0.20	0.20	0.30	0.30

<sup>1)</sup> For N, see Table 1.

Table 3. Structure of the ionic clusters  $\text{Ar}_k(\text{ArH})^+$  and ionic molecule  $(\text{ArH})^+$ . The distances (R) are in Å, the energies (E) in eV and the dipole moment ( $\mu$ ) in Debyes.

$\text{Ar}_k(\text{ArH})^+$	$q_{\text{H}}^{1)}$	$R_{\text{Ar-H}}^{2)}$	$R_{\text{Ar-Ar}}^{2)}$	$\mu$	E	Ar Detachment		
$(\text{ArH})^+$	0.569			2.78	-4.055			
$\text{Ar}(\text{ArH})^+$	0.579	2.81	3.70	5.98	-4.218	0.163		
$\text{Ar}_2(\text{ArH})^+$	0.591	2.79	3.81	6.32	-4.395	0.177		
$\text{Ar}_3(\text{ArH})^+$	0.601	2.79	3.72	6.23	-4.586	0.191		
$\text{Ar}_4(\text{ArH})^+$	0.609	2.84	3.57	4.94	-4.760	0.174		
$\text{Ar}_6(\text{ArH})^+$	0.614	2.84	3.17	3.87	3.38	3.33	-4.947	0.094

1) Charge of the H atom in  $(\text{ArH})^+$

2)  $R_{\text{Ar-H}}$  and  $R_{\text{Ar-Ar}}$  are the distances from the neutral atom to H and Ar of  $(\text{ArH})^+$ , respectively. For  $\text{Ar}_6(\text{ArH})^+$  there are two different Ar-H and Ar-Ar distances.

Table 4. Structure of the ionic clusters  $\text{Ar}_n\text{H}_2^+$  and ionic molecule  $\text{H}_2^+$ . The distances (R) are in Å, the energies in eV and the dipole moments ( $\mu$ ) in Debyes.

$\text{Ar}_n\text{H}_2^+$	$q_{\text{H}_2^+}$	$R_{\text{H-H}}$	$R_{\text{Ar}}$	$\mu$	E	Ar Detachment	T	Transitions		
								$\mu$	T	$\mu$
$\text{H}_2^+$	1.0	1.06		0	-2.790		11.8	2.5		
$\text{ArH}_2^+$	0.98	1.05	2.935	12.3	-2.983	0.193	5.65	1.9		
$\text{Ar}_2\text{H}_2^+$	0.964	1.05	2.94	9.02	-3.183	0.200	5.83	2.0		
$\text{Ar}_3\text{H}_2^+$	0.95	1.04	2.95	5.15	-3.377	0.194	5.58	0.8	5.89	2.3
$\text{Ar}_4\text{H}_2^+$	0.936	1.03	2.955	1.65	-3.568	0.191	5.71	0.9	5.94	2.5
$\text{Ar}_5\text{H}_2^+$	0.926	1.03	2.995	0	-3.754	0.186	5.44	1.7	5.92	2.2

1) Distance from the Ar atoms to the center of  $\text{H}_2^+$ . The adjacent Ar atoms are separated by 3.7 Å (n = 2-4) and 3.52 Å in symmetrical  $\text{Ar}_5\text{H}_2^+$ .

Table 5. Structure of the ionic clusters  $\text{Xe}_n^+$  and ionic molecule  $\text{Xe}_2^+$ . (See Table 1 for the footnotes.)

N	$\text{Xe}_n^+$	structure <sup>1)</sup>	R <sup>2)</sup>	R <sup>3)</sup>	q <sup>4)</sup>	E	Dissociation Products	D
I	$\text{Xe}_2^+$		3.22			-1.080	$\text{Xe}^+ + \text{Xe}$	1.08
II	$\text{Xe}_3^+$	linear	3.383			-1.277	$\text{Xe}_2^+ + \text{Xe}$	0.197
III	$\text{Xe}_4^+$	regular pyramid	3.646			-1.480	$\text{Xe}_2^+ + 2\text{Xe}$	0.40
IV	$\text{Xe}_4^+$	$(\text{Xe}_3^+)_z (\text{Xe})_{xz}$	3.384	4.19	0.014	-1.356	$\text{Xe}_3^+ + \text{Xe}$	0.079
V	$\text{Xe}_4^+$	linear	3.315	3.65	0.184	-1.346	$\text{Xe}_3^+ + \text{Xe}$	0.069
VI	$\text{Xe}_5^+$	$(\text{Xe}_4^+)_{\text{III}} (\text{Xe})_{xz}$	3.646	4.40	0.001	-1.568	$\text{Xe}_4^+ + \text{Xe}$	0.088
VII	$\text{Xe}_5^+$	$(\text{Xe}_3^+)_z (\text{Xe}_2)_{xz}$	3.383	4.24	0.005	-1.439	$\text{Xe}_3^+ \text{Xe} + \text{Xe}$	0.083
VIII	$\text{Xe}_6^+$	$(\text{Xe}_4^+)_{\text{III}} \text{Xe}_2$	3.644	4.40	0	-1.637	$\text{Xe}_4^+ \text{Xe} + \text{Xe}$	0.069
IX	$\text{Xe}_6^+$	$(\text{Xe}_3^+)_z (\text{Xe}_3)_{xz}$	3.375	4.20	0.021	-1.547	$\text{Xe}_3^+ \text{Xe}_2 + \text{Xe}$	0.108

Table 6. Transition energies T (eV) and moments  $\mu$ (D) of the  $\text{Xe}_3^+\text{Xe}_k$  allowed transitions.

N <sup>1)</sup>	$\text{Xe}_3^+\text{Xe}_k$	Transitions					
		T	$\mu$	T	$\mu$	T	$\mu$
II	$\text{Xe}_3^+$	1.87	11				
IV	$\text{Xe}_3^+\text{Xe}$	1.86	8.3	1.66	3.6	1.17	1.7
VII	$\text{Xe}_3^+\text{Xe}_2$	1.86	11			1.15	1.7
IX	$\text{Xe}_3^+\text{Xe}_3$	1.88	7.9	1.82	4.5	1.23	1.6

<sup>1)</sup> For N, see Table 6.

Table 7. Structure of the ionic clusters  $\text{Xe}_k(\text{XeH})^+$  and ionic molecule  $(\text{XeH})^+$ .

$\text{Xe}_k(\text{XeH})^+$	$q_{\text{H}}^{1)}$	$R_{\text{Xe-H}}^{2)}$	$R_{\text{Xe-Xe}^+}^{2)}$	$\mu$ (D)	E	Xe Detachment
$(\text{XeH})^+$	0.282			1.54	-4.050	
$\text{Xe}(\text{XeH})^+$	0.280	6.07	4.46	11.5	-4.096	0.046
$\text{Xe}_2(\text{XeH})^+$	0.279	5.95	4.50	12.7	-4.156	0.060
$\text{Xe}_3(\text{XeH})^+$	0.278	5.96	4.56	13.3	-4.235	0.079
$\text{Xe}_4(\text{XeH})^+$	0.277	5.91	4.62	12.4	-4.297	0.062
$\text{Xe}_5(\text{XeH})^+$	0.275	5.73	4.85	10.7	-4.372	0.038

1) Charge of the H atom in  $(\text{XeH})^+$ .

2)  $R_{\text{Xe-H}}$  and  $R_{\text{Xe-Xe}^+}$  are the distances from the neutral atom to H and Xe of  $(\text{XeH})^+$ , respectively.

### Figure Captions

- Fig. 1.  $\text{Ar}_3^+$  and  $\text{Ar}_4^+$  geometry. The Roman numerals indicate the clusters (the same as in Table 1). The numbers without a sign are distances in Å, and the numbers with the + sign are the atomic charges.
- Fig. 2. Geometry of the ionic clusters  $\text{Ar}(\text{ArH})^+$ ,  $\text{Ar}_2(\text{ArH})^+$  and  $\text{ArH}_2^+$ . For notations, see Fig. 1.
- Fig. 3. Geometry of  $\text{Xe}_3^+$  and  $\text{Xe}_4^+$ . For notations, see Fig. 1. The Roman numerals indicate the clusters (see Table 5).
- Fig. 4. Geometry of the ionic clusters  $\text{Xe}(\text{XeH})^+$ ,  $\text{Xe}_2(\text{XeH})^+$ ,  $(\text{XeH}_2)^+$  and  $\text{Xe}_2^+\text{H}_2$ . For notations, see Figs. 1 and 3.

Fig 1

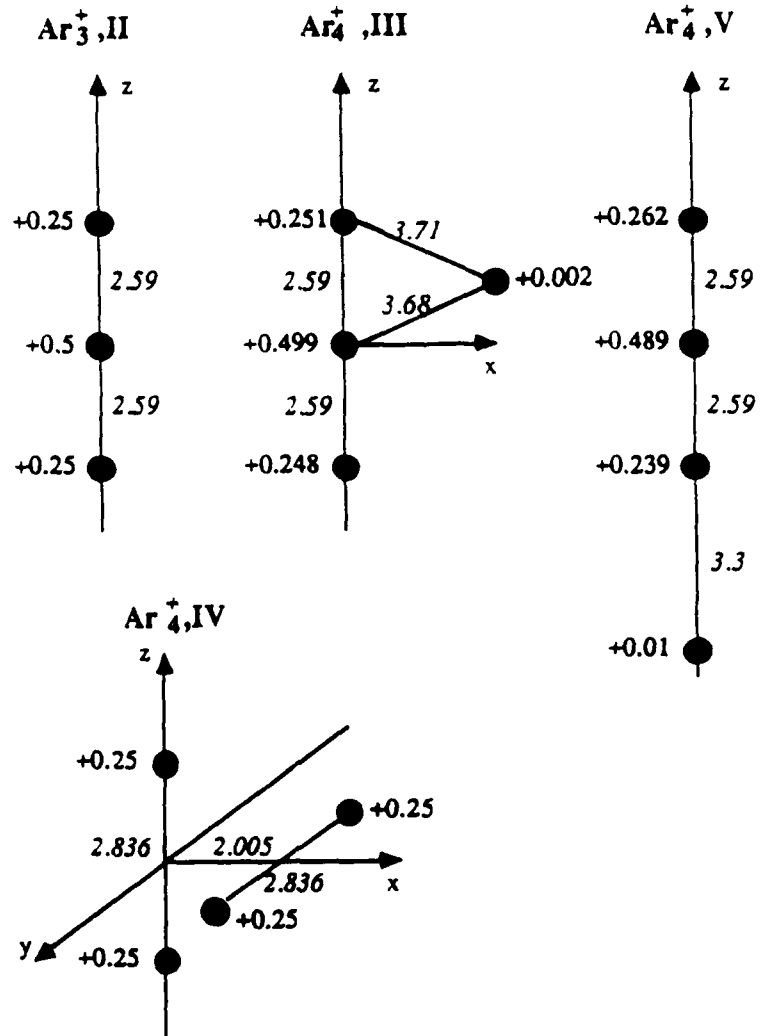
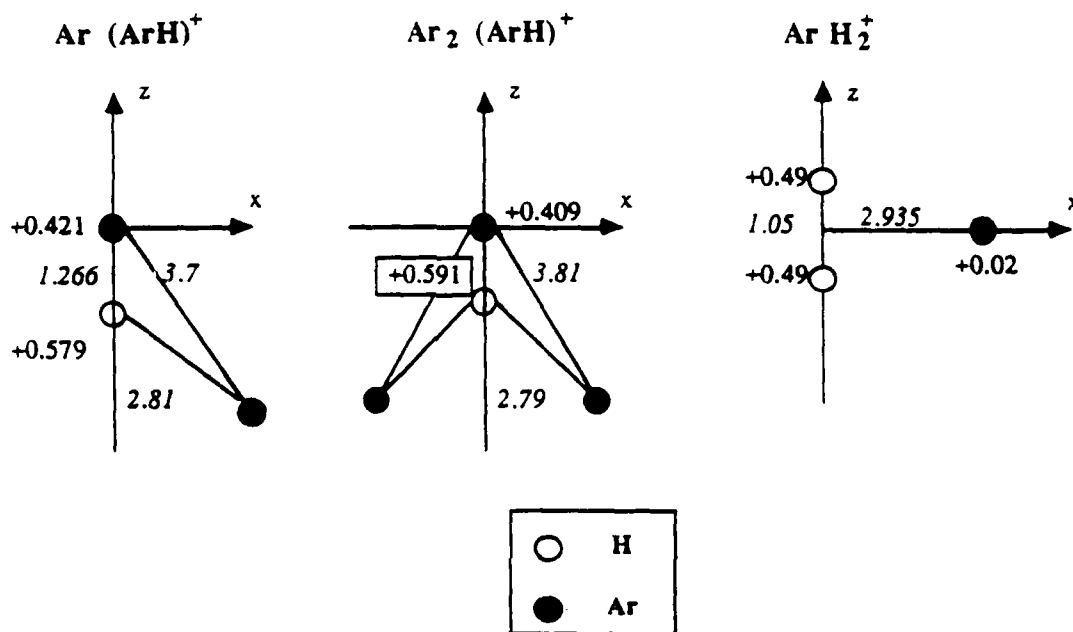


Fig. 2



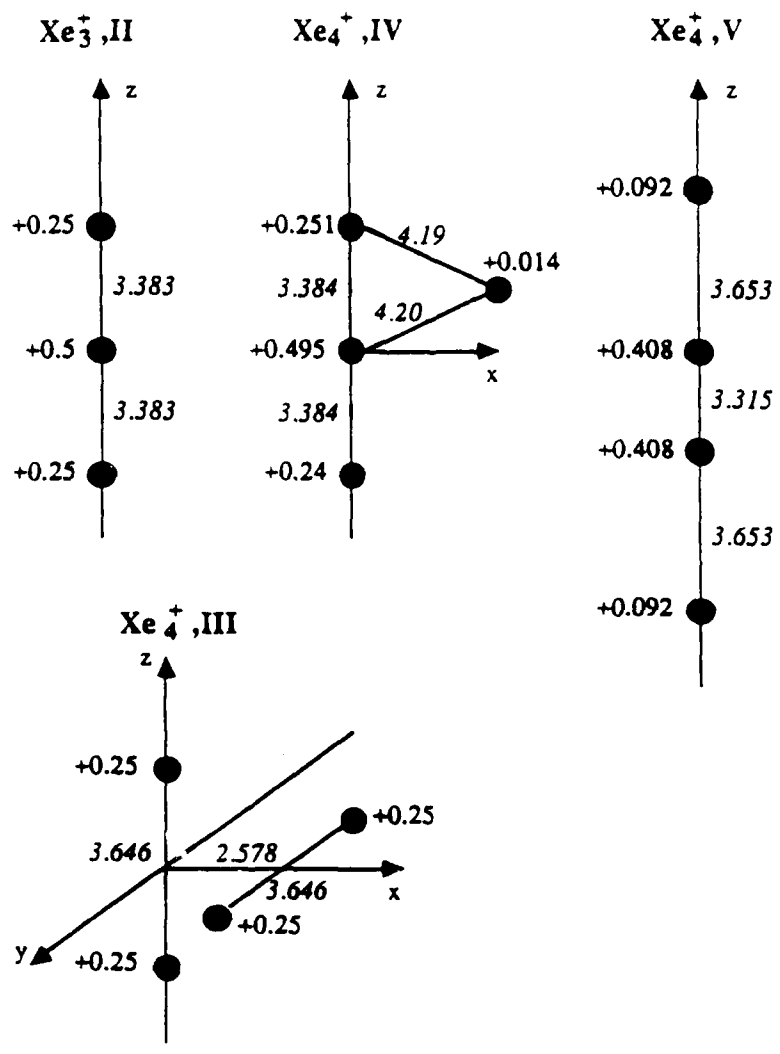
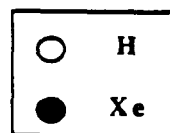
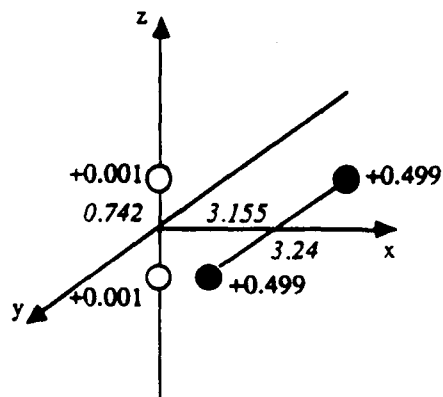
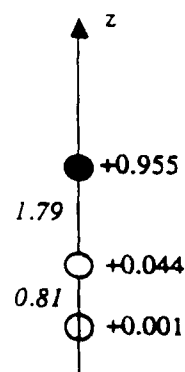
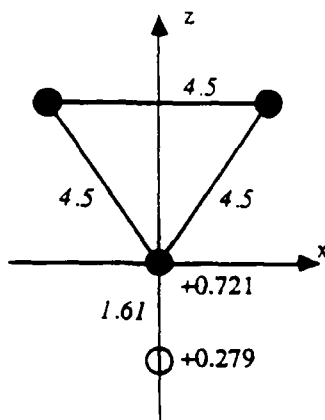
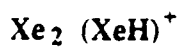
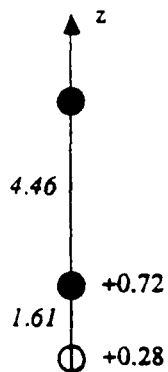
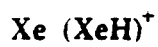


Fig. 4



TECHNICAL REPORT DISTRIBUTION LIST - GENERAL

Office of Naval Research (2)  
Chemistry Division, Code 1113  
800 North Quincy Street  
Arlington, Virginia 22217-5000

Commanding Officer (1)  
Naval Weapons Support Center  
Dr. Bernard E. Douda  
Crane, Indiana 47522-5050

Dr. Richard W. Drisko (1)  
Naval Civil Engineering  
Laboratory  
Code L52  
Port Hueneme, CA 93043

David Taylor Research Center (1)  
Dr. Eugene C. Fischer  
Annapolis, MD 21402-5067

Dr. James S. Murday (1)  
Chemistry Division, Code 6100  
Naval Research Laboratory  
Washington, D.C. 20375-5000

Dr. David L. Nelson (1)  
Chemistry Division  
Office of Naval Research  
800 North Quincy Street  
Arlington, Virginia 22217

Dr. Robert Green, Director (1)  
Chemistry Division, Code 385  
Naval Weapons Center  
China Lake, CA 93555-6001

Chief of Naval Research (1)  
Special Assistant for Marine  
Corps Matters  
Code 00MC  
800 North Quincy Street  
Arlington, VA 22217-5000

Dr. Bernadette Eichinger (1)  
Naval Ship Systems Engineering  
Station  
Code 053  
Philadelphia Naval Base  
Philadelphia, PA 19112

Dr. Sachio Yamamoto (1)  
Naval Ocean Systems Center  
Code 52  
San Diego, CA 92152-5000

Dr. Harold H. Singerman (1)  
David Taylor Research Center  
Code 283  
Annapolis, MD 21402-5067

Defense Technical Information Center (2)  
Building 5, Cameron Station  
Alexandria, VA 22314

FY90 Abstracts Distribution List for Solid State & Surface Chemistry

Professor John Baldeschwieler  
Department of Chemistry  
California Inst. of Technology  
Pasadena, CA 91125

Professor Paul Barbara  
Department of Chemistry  
University of Minnesota  
Minneapolis, MN 55455-0431

Dr. Duncan Brown  
Advanced Technology Materials  
520-B Danury Rd.  
New Milford, CT 06776

Professor Stanley Bruckenstein  
Department of Chemistry  
State University of New York  
Buffalo, NY 14214

Professor Carolyn Cassady  
Department of Chemistry  
Miami University  
Oxford, OH 45056

Professor R.P.H. Chang  
Dept. Matls. Sci. & Engineering  
Northwestern University  
Evanston, IL 60208

Professor Frank DiSalvo  
Department of Chemistry  
Cornell University  
Ithaca, NY 14853

Dr. James Duncan  
Federal Systems Division  
Eastman Kodak Company  
Rochester, NY 14650-2156

Professor Arthur Ellis  
Department of Chemistry  
University of Wisconsin  
Madison, WI 53706

Professor Mustafa El-Sayed  
Department of Chemistry  
University of California  
Los Angeles, CA 90024

Professor John Eyler  
Department of Chemistry  
University of Florida  
Gainesville, FL 32611

Professor James Garvey  
Department of Chemistry  
State University of New York  
Buffalo, NY 14214

Professor Steven George  
Department of Chemistry  
Stanford University  
Stanford, CA 94305

Professor Tom George  
Dept. of Chemistry & Physics  
State University of New York  
Buffalo, NY 14260

Dr. Robert Hamers  
IBM T.J. Watson Research Center  
P.O. Box 218  
Yorktown Heights, NY 10598

Professor Paul Hansma  
Department of Physics  
University of California  
Santa Barbara, CA 93106

Professor Charles Harris  
Department of Chemistry  
University of California  
Berkeley, CA 94720

Professor John Hemminger  
Department of Chemistry  
University of California  
Irvine, CA 92717

Professor Roald Hoffmann  
Department of Chemistry  
Cornell University  
Ithaca, NY 14853

Professor Leonard Interrante  
Department of Chemistry  
Rensselaer Polytechnic Institute  
Troy, NY 12181

Professor Eugene Irene  
Department of Chemistry  
University of North Carolina  
Chapel Hill, NC 27514

Dr. Sylvia Johnson  
SRI International  
333 Ravenswood Avenue  
Menlo Park, CA 94025

Dr. Zakya Kafafi  
Code 6551  
Naval Research Laboratory  
Washington, DC 20375-5000

Professor Larry Kesmodel  
Department of Physics  
Indiana University  
Bloomington, IN 47403

Professor Max Lagally  
Dept. Metal. & Min. Engineering  
University of Wisconsin  
Madison, WI 53706

Dr. Stephen Lieberman  
Code 522  
Naval Ocean Systems Center  
San Diego, CA 92152

Professor M.C. Lin  
Department of Chemistry  
Emory University  
Atlanta, GA 30322

Professor Fred McLafferty  
Department of Chemistry  
Cornell University  
Ithaca, NY 14853-1301

Professor Horia Metiu  
Department of Chemistry  
University of California  
Santa Barbara, CA 93106

Professor Larry Miller  
Department of Chemistry  
University of Minnesota  
Minneapolis, MN 55455-0431

Professor George Morrison  
Department of Chemistry  
Cornell University  
Ithaca, NY 14853

Professor Daniel Neumark  
Department of Chemistry  
University of California  
Berkeley, CA 94720

Professor David Ramaker  
Department of Chemistry  
George Washington University  
Washington, DC 20052

Dr. Gary Rubloff  
IBM T.J. Watson Research Center  
P.O. Box 218  
Yorktown Heights, NY 10598

Professor Richard Smalley  
Department of Chemistry  
Rice University  
P.O. Box 1892  
Houston, TX 77251

Professor Gerald Stringfellow  
Dept. of Matls. Sci. & Engineering  
University of Utah  
Salt Lake City, UT 84112

Professor Galen Stucky  
Department of Chemistry  
University of California  
Santa Barbara, CA 93106

Professor H. Tachikawa  
Department of Chemistry  
Jackson State University  
Jackson, MI 39217-0510

Professor William Unertl  
Lab. for Surface Sci. & Technology  
University of Maine  
Orono, ME 04469

Dr. Terrell Vanderah  
Code 3854  
Naval Weapons Center  
China Lake, CA 93555

Professor John Weaver  
Dept. of Chem. & Mat. Sciences  
University of Minnesota  
Minneapolis, MN 55455

Professor Brad Weiner  
Department of Chemistry  
University of Puerto Rico  
Rio Piedras, Puerto Rico 00931

Professor Robert Whetten  
Department of Chemistry  
University of California  
Los Angeles, CA 90024

Professor R. Stanley Williams  
Department of Chemistry  
University of California  
Los Angeles, CA 90024

Professor Nicholas Winograd  
Department of Chemistry  
Pennsylvania State University  
University Park, PA 16802

Professor Aaron Wold  
Department of Chemistry  
Brown University  
Providence, RI 02912

Professor Vicki Wysocki  
Department of Chemistry  
Virginia Commonwealth University  
Richmond, VA 23284-2006

Professor John Yates  
Department of Chemistry  
University of Pittsburgh  
Pittsburgh, PA 15260